

# Analysis of the Group Sparsity based on the Rank Minimization Methods

Zhiyuan Zha, Xinggan Zhang, Qiong Wang, Lan Tang and Xin Liu

**Abstract**—Sparse coding has achieved a great success in various image processing studies. However, there is not any benchmark to measure the sparsity of image patch/group because the sparse discriminant conditions cannot keep unchanged. This paper analyzes the sparsity of group based on the strategy of the rank minimization. Firstly, an adaptive dictionary is designed for each group. Then, we prove that group-based sparse coding is equivalent to the rank minimization problem, and thus the sparse coefficients of each group can be measured by estimating the singular values of each group. Based on that conclusion, four nuclear norm minimization methods including the standard nuclear norm minimization (NNM), the weighted nuclear norm minimization (WNNM), Schatten  $p$ -norm minimization (SNM) and the weighted Schatten  $p$ -norm minimization (WSNM) are used to analyze the sparsity of each group and WSNM is found to be the closest solution to the real singular values of each group. Therefore, WSNM can be equivalently turned into a non-convex weighted  $\ell_p$ -norm minimization problem in group-based sparse coding. To make the proposed scheme tractable and robust, the alternating direction method of multipliers (ADMM) is developed to solve the non-convex optimization problem. Experimental results on two low-level vision tasks: image inpainting and image compressive sensing (CS) recovery, show that the proposed scheme is feasible and outperforms existing state-of-the-art reconstruction methods both quantitatively and qualitatively.

**Index Terms**—Group sparsity, rank minimization, weighted Schatten  $p$ -norm, adaptive dictionary, ADMM.

## I. INTRODUCTION

Traditional patch-based sparse coding has been widely used in various image processing tasks [1–6]. It assumes that each patch of an image can be precisely modeled as a sparse linear combination of basis elements. These elements are called atoms and they compose a dictionary. As such, one key issue of sparse coding based scheme is to train a dictionary from natural images. Popular techniques are KSVD [1], ODL [5] and SDL [6]. Compared with the conventional analytically designed dictionaries, such as those based on DCT [7] and wavelet [8], dictionaries learned from images have an advantage of being better adapted to image local structures, and thus could improve the sparsity performance. For instance, the seminal of KSVD dictionary learning method [1] has not only displayed promising denoising performance, but also

been extended and successfully exploited in various image processing and computer vision tasks [9–11]. However, two main issues still existed for patch-based sparse coding model. On one hand, since dictionary learning is a large-scale and highly non-convex problem, it is computationally expensive to solve the sparsity optimization problem. On the other hand, the patch-based sparse coding model usually assumes the independence between sparsely coded patches, which takes no account of the correlation of similar patches in essence.

Instead of using patch as the basic unit of sparse coding, recent advances have suggested that, group-based sparse coding (GSC) has shown great potential in various image processing studies [12–15]. The GSC provides a powerful mechanism of combining local sparsity and nonlocal self-similarity of images simultaneously. Specifically, an image  $X$  with size  $N$  is divided into  $n$  overlapped patches of size  $\sqrt{d} \times \sqrt{d}$ , and each patch is denoted by the vector  $\mathbf{x}_i \in \mathbb{R}^d, i = 1, 2, \dots, n$ . Then for each patch  $\mathbf{x}_i$ , its  $m$  similar patches are selected from a  $L \times L$  sized search window to form a set  $\mathcal{S}_i$ . After this, all the patches in  $\mathcal{S}_i$  are stacked into a matrix  $\mathbf{X}_i \in \mathbb{R}^{d \times m}$ , which contains every element of  $\mathcal{S}_i$  as its column, i.e.,  $\mathbf{X}_i = \{\mathbf{x}_{i,1}, \mathbf{x}_{i,2}, \dots, \mathbf{x}_{i,m}\}$ . The matrix  $\mathbf{X}_i$  consisting of all the patches with similar structures is called a group, where  $\mathbf{x}_{i,m}$  denotes the  $m$ -th similar patch of the  $i$ -th group. Similar to patch-based sparse coding [1, 2], given a dictionary  $\mathbf{D}_i$ , each group  $\mathbf{X}_i$  can be sparsely represented as  $\boldsymbol{\alpha}_i = \mathbf{D}_i^{-1} \mathbf{X}_i$  and solved by the following  $\ell_0$ -norm minimization problem,

$$\boldsymbol{\alpha}_i = \arg \min_{\boldsymbol{\alpha}_i} \left( \frac{1}{2} \|\mathbf{X}_i - \mathbf{D}_i \boldsymbol{\alpha}_i\|_F^2 + \lambda \|\boldsymbol{\alpha}_i\|_0 \right) \quad (1)$$

where  $\lambda$  is the regularization parameter,  $\|\cdot\|_F^2$  denotes the Frobenious norm, and  $\|\cdot\|_0$  is  $\ell_0$ -norm, counting the nonzero entries of  $\boldsymbol{\alpha}_i$ .

However, since  $\|\cdot\|_0$  norm minimization is a difficult combinatorial optimization, solving Eq. (1) is NP-hard. For this reason, it is often replaced by the  $\ell_1$ -norm or the weighted  $\ell_1$ -norm [16] to make the optimization problem easy. Nonetheless, the solution of these norm minimizations is only the estimation of the real sparsity solution under certain conditions. For example, Candès *et al.* [17] proposed that solving  $\ell_1$ -norm optimization problem can recover a  $K$ -sparse signal  $\mathbf{x} \in \mathbb{R}^N$  from  $M = O(K \log(N/K))$  random measurements in compressive sensing (CS). However,  $\ell_1$ -norm minimization cannot still obtain the real sparsity solution, one important reason is that nobody can guarantee the invariance of sparse discriminant conditions. In other words, there is not any benchmark to measure the sparsity of a signal/image.

Z. Zha, X. Zhang and Q. Wang are with the department of Electronic Science and Engineering, Nanjing University, Nanjing 210023, China. E-mail: zhazhiyuan.mmd@gmail.com.

L. Tang is with the department of Electronic Science and Engineering, Nanjing University, and National Mobile Commun. Research Lab., Southeast University, Nanjing 210023, China.

L. Xin is with the Center for Machine Vision and Signal Analysis, University of Oulu, 90014, Finland. E-mail: linuxsino@gmail.com.

With the above consideration, in this paper we analyze the group sparsity from the point of the rank minimization. To the best of our knowledge, few works have exploited the rank minimization methods to analyze the sparsity of image group. The contribution of this paper is as follows. First, an adaptive dictionary for each group is designed with a low computational complexity, rather than dictionary learning from natural images. Second, based on this dictionary learning scheme, we prove the equivalence of group-based sparse coding and the rank minimization problem, and thus the sparse coefficients of each group are measured by calculating the singular values of each group. Therefore, we have a benchmark to measure the sparsity of each group because the singular values of the original image group can be easily computed by SVD operator. Third, we exploit four nuclear norm minimization methods (i.e., standard nuclear norm minimization (NNM) [18], the weighted nuclear norm minimization (WNNM) [19], Schatten  $p$ -norm minimization (SNM) [20] and the weighted Schatten  $p$ -norm minimization (WSNM) [21]) to analyze the sparsity of each group and the solution of WSNM is the nearest to real singular values of each group. Therefore, WSNM is equivalently translated into a non-convex weighted  $\ell_p$ -norm minimization problem in group-based sparse coding. We employ the proposed scheme on two low-level vision studies, including image inpainting and image compressive sensing (CS) recovery. Experimental results demonstrate that the proposed scheme is feasible and outperforms many existing state-of-the-art reconstruction methods.

The reminder of this paper is organized as follows. Section II briefly introduces the rank minimization method and some nuclear norms. Section III presents the adaptive dictionary learning method and analyzes the sparsity of each group based on the rank minimization methods. Section IV develops an efficient alternating direction method of multipliers (ADMM) method to solve the proposed scheme. Section V presents the experimental results. Finally, some concluding remarks are given in Section VI. The preliminary work has appeared in [22].

## II. BACKGROUND AND RELATED WORK

### A. Rank Minimization Method

The main goal of low rank matrix approximation (LRMA) is to recover the underlying low rank structure from its degraded/corrupted observation version. In general, methods of LRMA can be classified into two categories: the low rank matrix factorization (LRMF) methods [23–27] and the rank minimization methods [18–21]. Given an input data matrix  $\mathbf{Y}$ , the goal of LRMF is to factorize it into the product of two low rank matrices that can be used to reconstruct  $\mathbf{Y}$  under certain fidelity loss functions. A flurry of LRMF have been proposed, such as the classical singular value decomposition (SVD) under  $\ell_2$ -norm [23], robust LRMF methods under  $\ell_1$ -norm loss [24, 25], and other probabilistic methods [26, 27]. In this work we focus on the rank minimization problems. To be concrete, for an input matrix  $\mathbf{Y}$ , the rank minimization methods aim to find a low rank matrix  $\mathbf{X}$ , which is as close

to  $\mathbf{Y}$  as possible under  $F$ -norm data fidelity and one nuclear norm,

$$\hat{\mathbf{X}} = \arg \min_{\mathbf{X}} \left( \frac{1}{2} \|\mathbf{X} - \mathbf{Y}\|_F^2 + \lambda \mathbf{R}(\mathbf{X}) \right) \quad (2)$$

where  $\lambda$  is a trade-off parameter between the loss function and the low rank regularization induced by one nuclear norm  $\mathbf{R}(\mathbf{X})$ .

### B. Nuclear Norms

In this subsection, we will briefly introduce several nuclear norms, including standard nuclear norm [18], the weighted nuclear norm [19], Schatten  $p$ -norm [20] and the weighted Schatten  $p$ -norm [21].

We first introduce the weighted Schatten  $p$ -norm [21] of a matrix  $\mathbf{X} \in \Re^{m \times n}$ , which is defined as

$$\|\mathbf{X}\|_{\mathbf{w}, S_p} = \left( \sum_{i=1}^{\min\{m,n\}} w_i \sigma_i^p \right)^{\frac{1}{p}} \quad (3)$$

where  $0 < p \leq 1$ , and  $\sigma_i$  is the  $i$ -th singular value of  $\mathbf{X}$ .  $\mathbf{w} = [w_1, \dots, w_{\min\{m,n\}}]$  and  $w_i \geq 0$  is a non-negative weight assigned to  $\sigma_i$ . Then the weighted Schatten  $p$ -norm of  $\mathbf{X}$  with power  $p$  is

$$\|\mathbf{X}\|_{\mathbf{w}, S_p}^p = \sum_{i=1}^{\min\{m,n\}} w_i \sigma_i^p = \text{Tr}(\mathbf{W}\mathbf{\Delta}^p) \quad (4)$$

where  $\mathbf{W}$  and  $\mathbf{\Delta}$  are diagonal matrices whose diagonal entries are composed of  $w_i$  and  $\sigma_i$ , respectively.

The Schatten  $p$ -norm [20] of a matrix  $\mathbf{X}$  can be represented by setting  $\mathbf{w} = [1, 1, \dots, 1]$  in Eq. (3),

$$\|\mathbf{X}\|_{S_p} = \left( \sum_{i=1}^{\min\{m,n\}} \sigma_i^p \right)^{\frac{1}{p}} = \left( \text{Tr}((\mathbf{X}^T \mathbf{X})^{\frac{p}{2}}) \right)^{\frac{1}{p}} \quad (5)$$

The weighted nuclear norm [19] of a matrix  $\mathbf{X}$  can be represented by setting  $p=1$  in Eq. (3),

$$\|\mathbf{X}\|_{\mathbf{w}, * } = \left( \sum_{i=1}^{\min\{m,n\}} w_i \sigma_i \right) = \text{Tr}(\mathbf{W}\mathbf{\Delta}) \quad (6)$$

A widely used standard nuclear norm [18] of a matrix  $\mathbf{X}$  can be represented by setting  $p=1$  and  $\mathbf{w} = [1, 1, \dots, 1]$  in Eq. (3),

$$\|\mathbf{X}\|_* = \sum_{i=1}^{\min\{m,n\}} \sigma_i = \text{Tr}((\mathbf{X}^T \mathbf{X})^{\frac{1}{2}}) \quad (7)$$

## III. ANALYZING THE SPARSITY OF GROUP BASED ON THE RANK MINIMIZATION METHODS

Due to the fact that the sparse discriminant conditions cannot keep unchanged and  $\ell_0$ -norm minimization is NP-hard problem, there is not any benchmark to measure the sparsity of image group. In this subsection, we analyze the group sparsity from the point of the rank minimization. To this end, an adaptive dictionary for each group is designed with a low computational complexity, rather than dictionary learning from natural images. Based on this dictionary learning scheme, we prove that group-based sparse coding is equivalent to the rank minimization problems, i.e., the sparse coefficients of each group are measured by calculating the singular values of each group. Therefore, we have a benchmark to measure the sparsity of each group via the rank minimization methods,

since the singular values of the original image group can be easily obtained. In this way, we can achieve a clear visual comparison effect to analyze the sparsity of each group based on the rank minimization methods (See Fig. 1 and Fig. 2).

#### A. Adaptive dictionary learning

In this subsection, an adaptive dictionary learning method is designed, that is, for each group  $\mathbf{X}_i$ , its adaptive dictionary can be learned from its observation  $\mathbf{Y}_i \in \mathbb{R}^{d \times m}$ .

More specifically, we apply the singular value decomposition (SVD) to  $\mathbf{Y}_i$ ,

$$\mathbf{Y}_i = \mathbf{U}_i \boldsymbol{\Sigma}_i \mathbf{V}_i^T = \sum_{j=1}^{n_1} \boldsymbol{\sigma}_{i,j} \mathbf{u}_{i,j} \mathbf{v}_{i,j}^T \quad (8)$$

where  $\boldsymbol{\mu}_i = [\boldsymbol{\sigma}_{i,1}, \boldsymbol{\sigma}_{i,2}, \dots, \boldsymbol{\sigma}_{i,n_1}]$ ,  $n_1 = \min(d, m)$ ,  $\boldsymbol{\Sigma}_i = \text{diag}(\boldsymbol{\mu}_i)$  is a diagonal matrix whose non-zero elements are represented by  $\boldsymbol{\mu}_i$ , and  $\mathbf{u}_{i,j}, \mathbf{v}_{i,j}$  are the columns of  $\mathbf{U}_i$  and  $\mathbf{V}_i$ , respectively.

Also, we define each dictionary atom  $\mathbf{d}_{i,j}$  of the adaptive dictionary  $\mathbf{D}_i$  for each group  $\mathbf{Y}_i$  is as follows:

$$\mathbf{d}_{i,j} = \mathbf{u}_{i,j} \mathbf{v}_{i,j}^T, \quad j = 1, 2, \dots, n_1 \quad (9)$$

Finally, by learning an adaptive dictionary  $\mathbf{D}_i = [\mathbf{d}_{i,1}, \mathbf{d}_{i,2}, \dots, \mathbf{d}_{i,n_1}]$  from each group  $\mathbf{Y}_i$ . It can be seen that the proposed dictionary learning method is efficient since it only requires one SVD operator for each group.

#### B. Prove the equivalence of Group-based Sparse Coding and the Rank Minimization Problem

To prove that the group-based sparse coding is equivalent to the rank minimization problem, we firstly give two following lemmas.

**Lemma 1** The minimization problem

$$\mathbf{x} = \arg \min_{\mathbf{x}} \left( \frac{1}{2} \|\mathbf{x} - \mathbf{a}\|_2^2 + \tau \cdot \|\mathbf{x}\|_1 \right) \quad (10)$$

has a closed-form solution, which can be expressed as

$$\hat{\mathbf{x}} = \text{soft}(\mathbf{a}, \tau) = \text{sgn}(\mathbf{a}, \tau) \cdot \max(\text{abs}(\mathbf{a}) - \tau, 0) \quad (11)$$

*Proof:* see [28].

Consider the SVD of a matrix  $\mathbf{X} \in \mathbb{R}^{d \times m}$  of rank  $r$

$$\mathbf{X} = \mathbf{U} \boldsymbol{\Sigma} \mathbf{V}^T, \quad \boldsymbol{\Sigma} = \text{diag}(\{\sigma_i\}_{1 \leq i \leq r}) \quad (12)$$

where  $\mathbf{U} \in \mathbb{R}^{d \times r}$  and  $\mathbf{V} \in \mathbb{R}^{m \times r}$  are orthogonal matrices, respectively.  $\sigma_i$  is the  $i$ -th singular value of  $\mathbf{X}$ . For each  $\tau \geq 0$ , the soft-thresholding operator  $\mathcal{D}_\tau$  is defined as

$$\mathcal{D}_\tau(\mathbf{X}) = \mathbf{U} \mathcal{D}_\tau(\boldsymbol{\Sigma}) \mathbf{V}^T, \quad \mathcal{D}_\tau(\boldsymbol{\Sigma}) = \text{soft}(\sigma_i, \tau) \quad (13)$$

Then, we have the following Lemma.

**Lemma 2** For each  $\tau \geq 0$ , and  $\mathbf{Y} \in \mathbb{R}^{d \times m}$ , the singular value shrinkage operator Eq. (13) satisfies

$$\mathcal{D}_\tau(\mathbf{Y}) = \arg \min_{\mathbf{X}} \left( \frac{1}{2} \|\mathbf{X} - \mathbf{Y}\|_F^2 + \tau \|\mathbf{X}\|_* \right) \quad (14)$$

*Proof:* see [18].

Now, instead of Eq. (1), the classical  $\ell_1$ -norm group-based sparse coding problem can be represented as

$$\boldsymbol{\alpha}_i = \arg \min_{\boldsymbol{\alpha}_i} \left( \frac{1}{2} \|\mathbf{Y}_i - \mathbf{D}_i \boldsymbol{\alpha}_i\|_F^2 + \lambda \|\boldsymbol{\alpha}_i\|_1 \right) \quad (15)$$

According to the above design of adaptive dictionary  $\mathbf{D}_i$ , we have the following conclusion.

**Theorem 1**

$$\|\mathbf{Y}_i - \mathbf{X}_i\|_F^2 = \|\boldsymbol{\mu}_i - \boldsymbol{\alpha}_i\|_2^2 \quad (16)$$

where  $\mathbf{Y}_i = \mathbf{D}_i \boldsymbol{\mu}_i$  and  $\mathbf{X}_i = \mathbf{D}_i \boldsymbol{\alpha}_i$ .

The detailed proof of the Theorem 1 is given in the Appendix A.

Therefore, based on the Lemma 1, Lemma 2 and Theorem 1, we can prove the following theorem.

**Theorem 2**

The equivalence of the group-based sparse coding and the rank minimization problem is satisfied under the adaptive dictionary  $\mathbf{D}_i$ .

The detailed proof of the Theorem 2 is given in the Appendix B.

It can be similarly proven that the reweighted  $\ell_1$ -norm,  $\ell_p$ -norm and weighted  $\ell_p$ -norm are equivalent to the weighted nuclear norm [19], Schatten  $p$ -norm [20] and the weighted Schatten  $p$ -norm [21], respectively.

**Note that the main difference between sparse coding and the rank minimization problem is that sparse coding has a dictionary learning operator and the rank minimization problem does not involve.**

#### C. Analyzing the Sparsity of Group based on the Nuclear Norms Minimization

Based on Theorem 2, the group-based sparse coding can be turned into the rank minimization problem and the advantages of it are as follows. Since the sparse discriminant conditions cannot guarantee unchanged and  $\ell_0$ -norm minimization is NP-hard problem, there is not any benchmark to measure the sparsity of each group. However, we can possess a benchmark to measure the sparsity of each group by the rank minimization methods because the singular value of each group can be easily achieved. In this way, we can obtain a clear visual comparison effect to analyze the sparsity of each group based on the rank minimization methods.

Specifically, four nuclear norm minimization methods are used to constrain Eq. (2) to analyze the sparsity of each group, i.e., nuclear norm minimization (NNM) [18], the weighted nuclear norm minimization (WNNM) [19], Schatten  $p$ -norm minimization (SNM) [20] and the weighted Schatten  $p$ -norm minimization (WSNM) [21]. In these experiments, two gray images *Barbara* and *boats* are used as examples in the context of image inpainting and image CS recovery, respectively. In image inpainting, 80% pixels of image *Barbara* are damaged in Fig. 1(b) and two groups based on 1# position and 2# position are generated in Fig. 1(a). In image CS recovery, image *boats* is undersampled by a random Gaussian matrix with  $0.2N$  measurements and an initial image is estimated by using a standard CS recovery method (e.g., DCT/BCS [29] based recovery method) in Fig. 2(b). We conduct two groups

based on 3# position and 4# position in Fig. 2(a). As shown in Fig. 1(c), Fig. 1(d), Fig. 2(c) and Fig. 2(d), it can be seen that the singular values of WSNM result are the best approximation to the ground-truth in comparison with other three methods. Therefore, based on *Theorem 2*, WSNM can be equivalently transformed into solving the non-convex weighted  $\ell_p$ -norm minimization problem to measure the sparsity in group-based sparse coding.

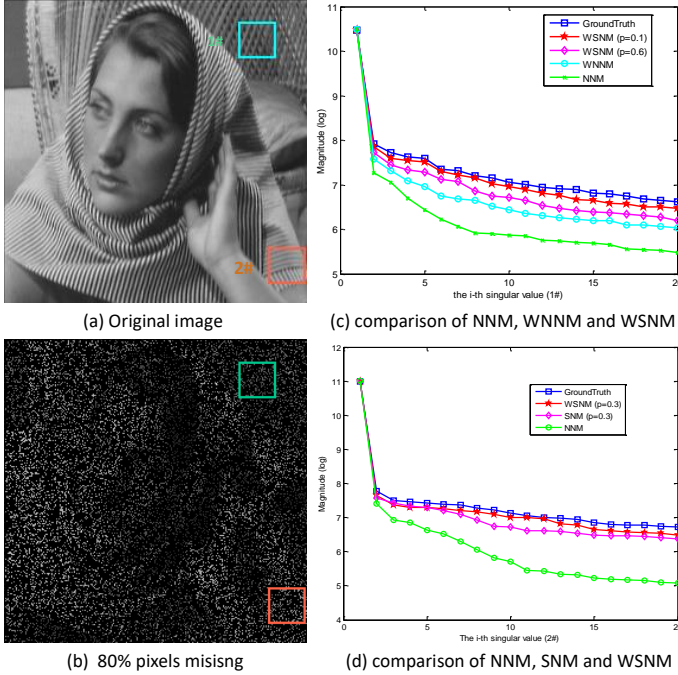


Fig. 1. Analyzing the sparsity of each group based nuclear norms minimization in terms of image inpainting.

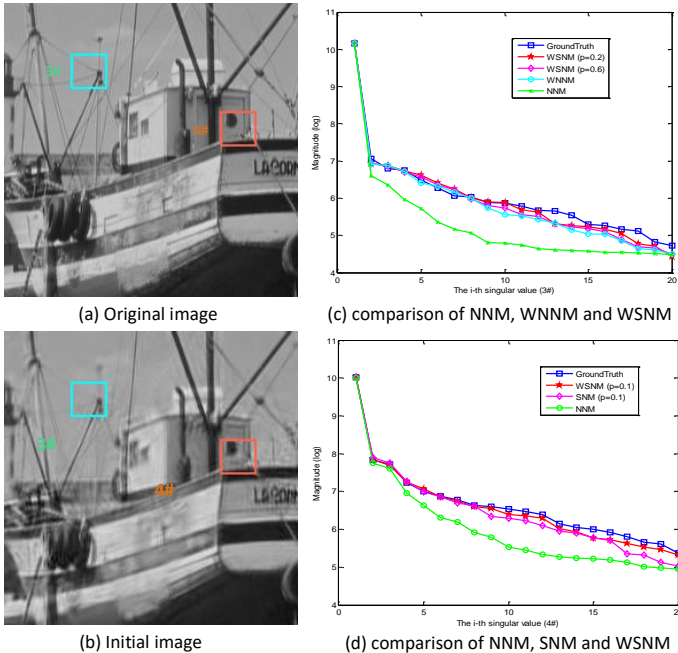


Fig. 2. Analyzing the sparsity of each group based nuclear norms minimization in terms of image CS recovery.

#### IV. GROUP-BASED SPARSE CODING FOR IMAGE RESTORATION WITH NON-CONVEX WEIGHTED $\ell_p$ -NORM MINIMIZATION

In this section, we verify the proposed scheme in the application of image restoration (IR). IR aims to reconstruct a high quality image  $X$  from its degraded observation  $Y$ ,

$$Y = HX + N \quad (17)$$

where  $H$  is a non-invertible linear degradation operator and  $N$  is usually assumed to be additive white Gaussian noise. With different setting of matrix  $H$ , Eq. (17) can represent different IR tasks. For instance, when  $H$  is an identity matrix, Eq. (17) becomes image denoising [30, 31]; when  $H$  is a blur operator, Eq. (17) becomes image deblurring [13, 14]; when  $H$  is a mask,  $H$  is a diagonal matrix whose diagonal entries are either 1 or 0, keeping or killing corresponding pixels, Eq. (17) becomes image inpainting [32]; when  $H$  is a random projection matrix, Eq. (17) becomes image compressive sensing (CS) recovery [33]. In this paper, we will focus on image inpainting and image CS recovery.

In the scenario of IR, what we observed is the degraded image  $Y$  via Eq. (17), and thus the goal is to exploit the proposed scheme to recover the original image  $X$  from  $Y$  by solving the following non-convex weighted  $\ell_p$ -norm minimization problem,

$$\alpha = \arg \min_{\alpha} \frac{1}{2} \|Y - H\alpha\|_2^2 + \lambda \|\alpha\|_p \quad (18)$$

where  $\lambda$  is a regularization parameter.

##### A. ADMM based for Non-Convex Weighted $\ell_p$ -norm Minimization

Solving the objective function of Eq. (18) is very difficult, since it is a large scale non-convex optimization problem. To make the optimization tractable, in this section, we present the alternating direction method of multipliers (ADMM) [34] to solve Eq. (18). The ADMM method is a powerful tool for numerous large scale optimization problems. The basic idea is to turn the unconstrained minimization problem into a constrained one by variable splitting scheme. Numerical simulations have shown that it can converge by only using a small memory footprint, which makes it very attractive for various large-scale optimization problems [35, 36]. We will give briefs to introduce the ADMM method by considering a constrained optimization,

$$\min_{Z \in \mathbb{R}^N, \alpha \in \mathbb{R}^M} f(Z) + g(\alpha), \quad s.t. \quad Z = G\alpha \quad (19)$$

where  $G \in \mathbb{R}^{M \times N}$  and  $f : \mathbb{R}^N \rightarrow \mathbb{R}$ ,  $g : \mathbb{R}^M \rightarrow \mathbb{R}$ . The ADMM works are shown in Table I.

Now, let us come back to Eq. (18) and show how to exploit ADMM method to solve it. We first turn Eq. (18) into another equivalent constrained form by introducing an auxiliary variable  $Z$ ,

$$\alpha = \arg \min_{Z, \alpha} \frac{1}{2} \|Y - HZ\|_2^2 + \lambda \|\alpha\|_p, \quad s.t. \quad Z = D\alpha \quad (20)$$

TABLE I  
THE ALTERNATING DIRECTION METHOD OF MULTIPLIERS (ADMM).

1. <b>Initialization</b> $t$ , choose $\rho > 0$ , $\mathbf{Z}$ , $\boldsymbol{\alpha}$ , and $\mathbf{b}$ .
2. <b>Repeat</b>
3. $\mathbf{Z}^{t+1} = \arg \min_{\mathbf{Z}} f(\mathbf{Z}) + \frac{\rho}{2} \ \mathbf{Z} - \mathbf{G}\boldsymbol{\alpha}^t - \mathbf{b}^t\ _2^2$ ;
4. $\boldsymbol{\alpha}^{t+1} = \arg \min_{\boldsymbol{\alpha}} g(\boldsymbol{\alpha}) + \frac{\rho}{2} \ \mathbf{Z}^{t+1} - \mathbf{G}\boldsymbol{\alpha} - \mathbf{b}^t\ _2^2$ ;
5. $\mathbf{b}^{t+1} = \mathbf{b}^t - (\mathbf{Z}^{t+1} - \mathbf{G}\boldsymbol{\alpha}^{t+1})$ ;
6. $t \leftarrow t + 1$ ;
7. <b>Until</b> stopping criterion is satisfied.

Accordingly, based on the ADMM method, Eq. (18) can be transformed into three iterative steps:

$$\mathbf{Z}^{t+1} = \arg \min_{\mathbf{Z}} \frac{1}{2} \|\mathbf{Y} - \mathbf{H}\mathbf{Z}\|_2^2 + \frac{\rho}{2} \|\mathbf{Z} - \mathbf{D}\boldsymbol{\alpha}^t - \mathbf{b}^t\|_2^2 \quad (21)$$

$$\boldsymbol{\alpha}^{t+1} = \arg \min_{\boldsymbol{\alpha}} \lambda \|\mathbf{w}\boldsymbol{\alpha}\|_p + \frac{\rho}{2} \|\mathbf{Z}^{t+1} - \mathbf{D}\boldsymbol{\alpha} - \mathbf{b}^t\|_2^2 \quad (22)$$

and

$$\mathbf{b}^{t+1} = \mathbf{b}^t - (\mathbf{Z}^{t+1} - \mathbf{D}\boldsymbol{\alpha}^{t+1}) \quad (23)$$

One can observe that the minimization for Eq. (18) involves splitting two minimization sub-problems, i.e.,  $\mathbf{Z}$  and  $\boldsymbol{\alpha}$  sub-problems. Next, we will show that there is an efficient solution to each sub-problem. To avoid confusion, the subscribe  $t$  may be omitted for conciseness.

1) **Z Sub-problem:** Given  $\boldsymbol{\alpha}$ , the  $\mathbf{Z}$  sub-problem denoted by Eq. (21) becomes

$$\min_{\mathbf{Z}} L_1(\mathbf{Z}) = \min_{\mathbf{Z}} \frac{1}{2} \|\mathbf{Y} - \mathbf{H}\mathbf{Z}\|_2^2 + \frac{\rho}{2} \|\mathbf{Z} - \mathbf{D}\boldsymbol{\alpha} - \mathbf{b}\|_2^2 \quad (24)$$

Obviously, one can observe that the above minimization problem has a closed-form solution. Thus, we have

$$\hat{\mathbf{Z}} = (\mathbf{H}^T \mathbf{H} + \rho \mathbf{I})^{-1} (\mathbf{H}^T \mathbf{Y} + \rho(\mathbf{D}\boldsymbol{\alpha} + \mathbf{b})) \quad (25)$$

where  $\mathbf{I}$  is the identity matrix.

Owing to the specific structure of  $\mathbf{H}$  in image inpainting, Eq. (24) can be efficiently computed without computing the matrix inverse (more details can be seen in [37]).

However, since  $\mathbf{H}$  is a random projection matrix without a specific structure in image CS recovery, it is too costly to solve Eq. (24) directly by Eq. (25). Therefore, to avoid computing the matrix inverse, an iterative algorithm is highly desired for solving Eq. (24). In this work, we adopt the gradient descent method [38] with an optimal step to solve Eq. (24),

$$\hat{\mathbf{Z}} = \mathbf{Z} - \eta \mathbf{q} \quad (26)$$

where  $\mathbf{q}$  is the gradient direction of the objective function  $L_1(\mathbf{Z})$ , and  $\eta$  is the optimal step.

Accordingly, in image CS recovery, it only requires an iterative calculation of the following equation to solve the  $\mathbf{Z}$  sub-problem,

$$\hat{\mathbf{Z}} = \mathbf{Z} - \eta (\mathbf{H}^T \mathbf{H} \mathbf{Z} - \mathbf{H}^T \mathbf{Y} + \rho(\mathbf{Z} - \mathbf{D}\boldsymbol{\alpha} - \mathbf{b})) \quad (27)$$

where  $\mathbf{H}^T \mathbf{H}$  and  $\mathbf{H}^T \mathbf{Y}$  can be calculated in advance.

2)  **$\boldsymbol{\alpha}$  sub-problem:** Given  $\mathbf{Z}$ , similarity, according to Eq. (22), the  $\boldsymbol{\alpha}$  sub-problem can be rewritten as

$$\min_{\boldsymbol{\alpha}} L_2(\boldsymbol{\alpha}) = \min_{\boldsymbol{\alpha}} \frac{1}{2} \|\mathbf{D}\boldsymbol{\alpha} - \mathbf{R}\|_2^2 + \frac{\lambda}{\rho} \|\mathbf{w}\boldsymbol{\alpha}\|_p \quad (28)$$

where  $\mathbf{R} = \mathbf{Z} - \mathbf{b}$ .

However, due to the complex structure of  $\|\mathbf{w}\boldsymbol{\alpha}\|_p$ , it is difficult to solve Eq. (28). Let  $\mathbf{X} = \mathbf{D}\boldsymbol{\alpha}$ , Eq. (28) can be rewritten as

$$\min_{\boldsymbol{\alpha}} L_2(\boldsymbol{\alpha}) = \min_{\boldsymbol{\alpha}} \frac{1}{2} \|\mathbf{X} - \mathbf{R}\|_2^2 + \frac{\lambda}{\rho} \|\mathbf{w}\boldsymbol{\alpha}\|_p \quad (29)$$

To enable a tractable solution of Eq. (29), in this paper, a general assumption is made, with which even a closed-form solution can be achieved. Specifically,  $\mathbf{R}$  can be regarded as some type of noisy observation of  $\mathbf{X}$ , and then the assumption is made that each element of  $\mathbf{E} = \mathbf{X} - \mathbf{R}$  follows an independent zero-mean distribution with variance  $\sigma^2$ . The following conclusion can be proved by this assumption.

**Theorem 3** Define  $\mathbf{X}, \mathbf{R} \in \mathbb{R}^N$ ,  $\mathbf{X}_i, \mathbf{R}_i$ , and  $\mathbf{e}(j)$  as each element of error vector  $\mathbf{e}$ , where  $\mathbf{e} = \mathbf{X} - \mathbf{R}, j = 1, \dots, N$ . Assume that  $\mathbf{e}(j)$  follows an independent zero mean distribution with variance  $\sigma^2$ , and thus for any  $\varepsilon > 0$ , we can represent the relationship between  $\frac{1}{N} \|\mathbf{X} - \mathbf{R}\|_2^2$  and  $\frac{1}{S} \sum_{i=1}^n \|\mathbf{X}_i - \mathbf{R}_i\|_2^2$  by the following property,

$$\lim_{\substack{N \rightarrow \infty \\ K \rightarrow \infty}} \mathbf{P} \left( \left| \frac{1}{N} \|\mathbf{X} - \mathbf{R}\|_2^2 - \frac{1}{S} \sum_{i=1}^n \|\mathbf{X}_i - \mathbf{R}_i\|_F^2 \right| < \varepsilon \right) = 1 \quad (30)$$

where  $\mathbf{P}(\bullet)$  represents the probability and  $S = d \times m \times n$ .

The detailed proof of the Theorem 3 is given in the Appendix C.

Based on Theorem 3, we have the following equation with a very large probability (limited to 1) at each iteration,

$$\frac{1}{N} \|\mathbf{X} - \mathbf{R}\|_2^2 = \frac{1}{S} \sum_{i=1}^n \|\mathbf{X}_i - \mathbf{R}_i\|_F^2 \quad (31)$$

Based on Eqs. (29) and (31), we have

$$\begin{aligned} & \min_{\boldsymbol{\alpha}} \frac{1}{2} \|\mathbf{X} - \mathbf{R}\|_2^2 + \frac{\lambda}{\rho} \|\mathbf{w}\boldsymbol{\alpha}\|_p \\ &= \min_{\boldsymbol{\alpha}_i} \left( \sum_{i=1}^n \frac{1}{2} \|\mathbf{X}_i - \mathbf{R}_i\|_F^2 + \tau_i \|\mathbf{w}_i \boldsymbol{\alpha}_i\|_p \right) \\ &= \min_{\boldsymbol{\alpha}_i} \left( \sum_{i=1}^n \frac{1}{2} \|\mathbf{R}_i - \mathbf{D}_i \boldsymbol{\alpha}_i\|_F^2 + \tau_i \|\mathbf{w}_i \boldsymbol{\alpha}_i\|_p \right) \end{aligned} \quad (32)$$

where  $\tau_i = \lambda_i S / \rho N$  and  $\mathbf{D}_i$  is a dictionary. Clearly, Eq. (32) can be viewed as a sparse coding problem by solving  $n$  sub-problems for all the group  $\mathbf{X}_i$ . Based on Theorem 1, Eq. (32) can be rewritten as:

$$\hat{\boldsymbol{\alpha}}_i = \min_{\boldsymbol{\alpha}_i} \sum_{i=1}^n \left( \frac{1}{2} \|\boldsymbol{\gamma}_i - \boldsymbol{\alpha}_i\|_2^2 + \tau_i \|\mathbf{w}_i \boldsymbol{\alpha}_i\|_p \right) \quad (33)$$

where  $\mathbf{R}_i = \mathbf{D}_i \boldsymbol{\gamma}_i$  and  $\mathbf{X}_i = \mathbf{D}_i \boldsymbol{\alpha}_i$ .

Therefore, the minimization problem of Eq. (28) can be simplified by minimizing the problem of Eq. (33).

### B. Generalized Soft-Thresholding (GST) Algorithm for Non-Convex Optimization Problem

To obtain the solution of Eq. (33) effectively, in this subsection, the generalized soft-thresholding (GST) algorithm [39] is used to solve Eq. (33). More specifically, given  $p$ ,  $\gamma_{i,j}$  and  $w_{i,j}$ , there exists a specific threshold,

$$\tau_p^{GST}(w_{i,j}) = (2w_{i,j}(1-p))^{\frac{1}{2-p}} + w_{i,j}p(2w_{i,j}(1-p))^{\frac{p-1}{2-p}} \quad (34)$$

where  $\gamma_{i,j}$ ,  $\alpha_{i,j}$  and  $w_{i,j}$  are the  $j$ -th elements of  $\gamma_i$ ,  $\alpha_i$  and  $w_i$ , respectively. Then, if  $\gamma_{i,j} < \tau_p^{GST}(w_{i,j})$ ,  $\alpha_{i,j} = 0$  is the global minimum. Otherwise, the optimum will be obtained at non-zero point. According to [39], for any  $\gamma_{i,j} \in (\tau_p^{GST}(w_{i,j}), +\infty)$ , Eq. (33) has one unique minimum  $T_p^{GST}(\gamma_{i,j}; w_{i,j})$ , which can be obtained by solving the following equation,

$$T_p^{GST}(\gamma_{i,j}; w_{i,j}) - \gamma_{i,j} + w_{i,j}p(T_p^{GST}(\gamma_{i,j}; w_{i,j}))^{p-1} = 0 \quad (35)$$

The complete description of the GST algorithm is exhibited in Table II. For more details about the GST algorithm, please refer to [39].

TABLE II  
GENERALIZED SOFT-THRESHOLDING (GST) [39].

<b>Input:</b>	$\gamma_{i,j}, w_{i,j}, p, K$ .
1.	$\tau_p^{GST}(w_{i,j}) = (2w_{i,j}(1-p))^{\frac{1}{2-p}} + w_{i,j}p(2w_{i,j}(1-p))^{\frac{p-1}{2-p}}$ ;
2.	<b>If</b> $ \gamma_{i,j}  \leq \tau_p^{GST}(w_{i,j})$
3.	$T_p^{GST}(\gamma_{i,j}; w_{i,j}) = 0$ ;
4.	<b>else</b>
5.	$k = 0, \alpha_{i,j}^{(k)} =  \gamma_{i,j} $ ;
6.	Iterate on $k = 0, 1, \dots, K$
7.	$\alpha_{i,j}^{(k+1)} =  \gamma_{i,j}  - w_{i,j}p(\alpha_{i,j}^{(k)})^{p-1}$ ;
8.	$k \leftarrow k + 1$ ;
9.	$T_p^{GST}(\gamma_{i,j}; w_{i,j}) = \text{sgn}(\gamma_{i,j})\alpha_{i,j}^{(k)}$ ;
10.	<b>End</b>
<b>Output:</b>	$T_p^{GST}(\gamma_{i,j}; w_{i,j})$ .

Therefore, a closed-form solution of Eq. (33) can be computed as

$$\alpha_{i,j} = GST(\gamma_{i,j}, \tau w_{i,j}, p, K) \quad (36)$$

where  $K$  denotes the iteration number of the GST algorithm.

### C. Setting the Weight and Regularization Parameter

Inspired by [16], for each weight  $w_i$ , large values of each group sparse coefficient  $\alpha_i$  usually depict major edge and texture information. In other words, to reconstruct  $X_i$  from its degraded one, we should shrink the larger values less, while shrinking smaller ones more. Therefore, we let

$$w_i = \frac{1}{|\gamma_i| + \epsilon} \quad (37)$$

where  $\epsilon$  is a small constant.

The regularization parameter  $\lambda$  that balances the fidelity term and the regularization term should be adaptively determined for better reconstruction performance. Inspired by [40], the regularization parameter  $\lambda_i$  of each group  $R_i$  is set as:

$$\lambda_i = \frac{2\sqrt{2}\sigma^2}{\delta_i + \epsilon} \quad (38)$$

where  $\delta_i$  denotes the estimated variance of  $\gamma_i$ , and  $\epsilon$  is a small constant.

After solving the two sub-problems, we summarize the overall algorithm for Eq. (18) in Table III.

TABLE III  
ADMM METHOD FOR THE PROPOSED SCHEME.

<b>Input:</b>	the observed image $Y$ and the measurement matrix $H$ .
<b>Initialization:</b>	$t, b, Z, \alpha, L, K, d, m, \rho, p, \sigma, \epsilon$ and $\epsilon$ ;
<b>Repeat</b>	
<b>If</b> $H$ is mask operator.	Update $Z^{t+1}$ by Eq. (25);
<b>Else</b> $H$ is random projection operator.	Update $Z^{t+1}$ Eq. (27);
<b>End if</b>	$R^{t+1} = Z^{t+1} - b^t$ ;
<b>For</b>	Each group $R_i$ ;
Construct dictionary $D_i$ by computing Eq. (9);	
Update $\lambda_i^{t+1}$ by computing Eq. (38);	
Update $\tau_i^{t+1}$ computing by $\tau_i = \lambda_i K / \rho N$ ;	
Update $w_i^{t+1}$ by computing Eq. (37);	
Update $\alpha_i^{t+1}$ computing by Eq. (36);	
<b>End For</b>	Update $D^{t+1}$ by concatenating all $D_i$ ;
	Update $\alpha^{t+1}$ by concatenating all $\alpha_i$ ;
	Update $b^{t+1}$ by computing Eq. (23) ;
	$t \leftarrow t + 1$ ;
<b>Until</b>	maximum iteration number is reached.
<b>Output:</b>	The final restored image $\hat{X} = D\hat{\alpha}$ .

## V. EXPERIMENTAL RESULTS

To demonstrate the feasibility of the proposed scheme, in this section, we report extensive experiments to evaluate the performance of the non-convex weighted  $\ell_p$ -norm ( $w\ell_p$ -norm) minimization and compare it with many existing norm minimization methods, including  $\ell_1$ -norm minimization, weighted  $\ell_1$ -norm ( $w\ell_1$ -norm) minimization, and  $\ell_p$ -norm minimization in group-based sparse coding. We conduct performance evaluations on two low-level vision tasks, including image inpainting and image CS recovery. The objective image quality metric, peak signal-to-noise ratio (PSNR), is adopted to evaluate the quality of restored images. All experimental images are shown in Fig. 3.



Fig. 3. All experimental test images. Up: Mickey, Barbara, Butterfly, elaine, Fence, straw, Golem, peppers. Down: House, starfish, Fence, Nanna, lena, fireman, bridge, Zebra.

### A. Parameter Selection

The parameters used in the algorithm are empirically chosen according to the different scene in order to achieve relatively

good performance. Note that all norm minimization problems are based on the proposed adaptive dictionary learning (ADL) scheme in group-based sparse coding. The parameters are set as follows.

In image inpainting, the mask is conducted by the partial random samples. The size of each patch  $\sqrt{d} \times \sqrt{d}$  is set to be  $8 \times 8$ . The similar patch numbers  $m$  is set to be 60. The search window  $L \times L$  is set as  $25 \times 25$ .  $\sigma = \sqrt{2}$  and  $K = 2$ .  $p$  are set to 0.45, 0.45, 0.95 and 0.95 when 80%, 70%, 60% and 50% pixels missing, respectively.  $\epsilon$  and  $\varepsilon$  are set as 0.35, 0.35 and 0.1, 0.3 for  $wl_1$ -norm and  $wl_p$ -norm, respectively. The detailed setting of the involved parameters  $\rho$  and  $\lambda$  are shown in Table IV. However, due to the existence of the weight  $w$ ,  $\lambda$  is computed by Eq. (38) in  $wl_1$ -norm and  $wl_p$ -norm.

In image CS recovery, we generate the CS measurements at the block level by utilizing a Gaussian random projection matrix to test images, i.e., the CS recovery with block size  $32 \times 32$  [29]. The size of each patch  $\sqrt{d} \times \sqrt{d}$  is set to be  $7 \times 7$ . The similar patch numbers  $m = 60$ ,  $L = 20$ ,  $\sigma = \sqrt{2}$  and  $K = 2$ .  $p$  are set to 0.5, 0.95, 0.95 and 0.95 when  $0.2N$ ,  $0.3N$ ,  $0.4N$  and  $0.5N$  measurements, respectively.  $\epsilon$  and  $\varepsilon$  are set as 0.35, 0.35 and 0.1, 0.4 for  $wl_1$ -norm and  $wl_p$ -norm, respectively. Similarly, due to the existence of the weight  $w$ ,  $\lambda$  is computed by Eq. (38) in  $wl_1$ -norm and  $wl_p$ -norm. The detailed setting of the involved parameters  $\rho$  and  $\lambda$  are shown in Table IV.

In addition, to make a fair comparison of all norm minimization methods, The iterative stopping criterion is set as:  $\text{PSNR}(t+1) - \text{PSNR}(t) < 0$ , where  $\text{PSNR}(t+1)$  and  $\text{PSNR}(t)$  denotes the PSNR values of the  $t+1$ -th iteration and  $t$ -th iteration, respectively.

TABLE IV  
THE DETAILED INVOLVED PARAMETERS SETTING OF  $\rho$ ,  $\lambda$  FOR IMAGE INPAINTING AND IMAGE CS RECOVERY, BASED ON THE ADAPTIVE DICTIONARY LEARNING METHOD.

Image Inpainting						
ADL	$\ell_1$ -norm		$\ell_p$ -norm		$wl_1$ -norm	$wl_p$ -norm
Parameters	$\rho$	$\lambda$	$\rho$	$\lambda$	$\rho$	$\rho$
80%	7e-5	5e-6	0.006	0.07	0.1	0.0003
70%	1e-4	7e-6	0.008	0.07	0.1	0.0003
60%	1e-5	1e-6	7e-5	3e-6	0.1	0.03
50%	5e-5	1e-5	0.0001	7e-6	0.1	0.04
Image CS Recovery						
ADL	$\ell_1$ -norm		$\ell_p$ -norm		$wl_1$ -norm	$wl_p$ -norm
Parameters	$\rho$	$\lambda$	$\rho$	$\lambda$	$\rho$	$\rho$
0.2	0.001	5e-5	0.003	5e-4	0.1	0.0005
0.3	0.003	7e-4	0.01	3e-4	0.1	0.05
0.4	0.003	5e-4	0.006	3e-4	0.1	0.05
0.5	0.003	5e-4	0.006	3e-4	0.2	0.05

### B. Comparisons of $\ell_1$ -norm, weighted $\ell_1$ -norm, $\ell_p$ -norm and the weighted $\ell_p$ -norm

In this subsection, to verify the feasibility of the proposed scheme, we firstly have compared four norm minimization methods, i.e.,  $\ell_1$ -norm minimization, weighted  $\ell_1$ -norm minimization,  $\ell_p$ -norm minimization and weighted  $\ell_p$ -norm minimization, based on the proposed adaptive dictionary learning scheme for image inpainting and image CS recovery.

The PSNR results of image inpainting and image CS recovery are shown in Table V and Table VI, respectively. It can

be seen that the weighted  $\ell_p$ -norm can achieve better results than other three norms in most cases in terms of PSNR. Fig. 4 shows the image inpainting results of image *Mickey* with 80% pixels missing. Fig. 5 shows the image CS recovery results of image *straw* with  $0.2N$  measurements. One can observe that the weighted  $\ell_p$ -norm obtains better perceptual quality than other three norms. Therefore, it is quite clear that these experimental results are almost consistent with our previous theoretical analysis.

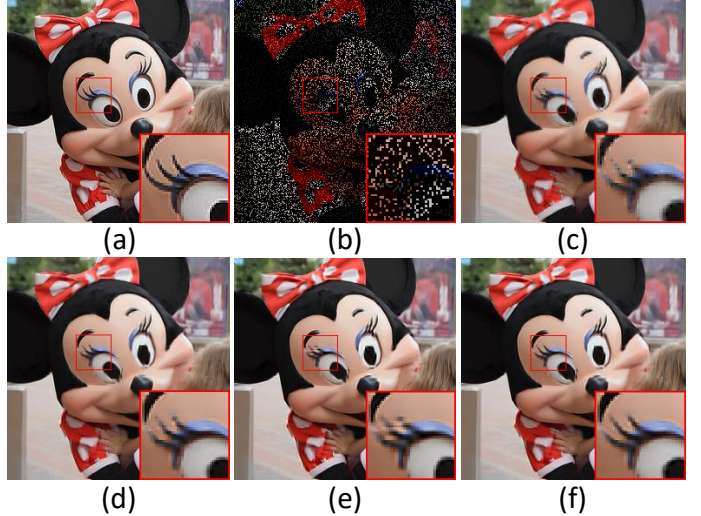


Fig. 4. Inpainting performance comparison on the image *Mickey* based on the adaptive dictionary learning method. (a) Original image; (b) Degraded image with 80% pixels missing sample; (c)  $\ell_1$ -norm (PSNR= 25.97dB); (d)  $\ell_p$ -norm (PSNR= 26.74dB); (e)  $wl_1$ -norm (PSNR= 26.66dB); (f)  $wl_p$ -norm (PSNR= 26.92dB).

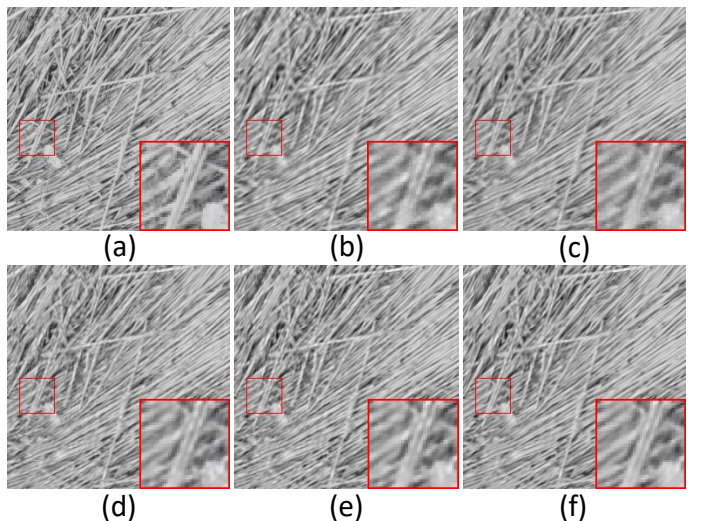


Fig. 5. CS recovery performance comparison on the image *straw* based on the adaptive dictionary learning method. (a) Original image; (b) Initial image by [29] (PSNR= 23.76dB); (c)  $\ell_1$ -norm (PSNR= 24.11dB); (d)  $\ell_p$ -norm (PSNR= 24.82dB); (e)  $wl_1$ -norm (PSNR= 24.82dB); (f)  $wl_p$ -norm (PSNR= 25.06dB).

To prove the universality of the proposed scheme, instead of using the proposed ADL method, we exploit another two more general dictionary learning methods to verify the feasibility of the proposed scheme, i.e., graph-based dictionary learning

TABLE V

PSNR (dB) COMPARISON OF  $\ell_1$ -NORM,  $\ell_p$ -NORM,  $w\ell_1$ -NORM AND  $w\ell_p$ -NORM, BASED ON THE ADAPTIVE DICTIONARY LEARNING SCHEME FOR IMAGE INPAINTING.

Miss pixels	Methods	Mickey	Butterfly	Fence	Starfish	Nanna	Zebra	fireman	Golem	Average
80%	$\ell_1$ -norm	25.97	25.61	28.90	26.98	25.46	22.33	25.39	25.29	25.74
	$\ell_p$ -norm	26.74	26.36	29.47	27.54	25.87	23.05	25.63	25.69	26.29
	$w\ell_1$ -norm	26.66	26.39	29.98	28.00	25.73	22.39	25.68	26.12	26.37
	$w\ell_p$ -norm	<b>26.92</b>	<b>26.52</b>	<b>30.00</b>	<b>28.05</b>	<b>25.95</b>	<b>23.06</b>	<b>25.80</b>	<b>26.26</b>	<b>26.57</b>
70%	$\ell_1$ -norm	27.86	27.86	30.72	29.02	27.32	24.26	27.05	27.40	27.69
	$\ell_p$ -norm	29.04	29.10	31.54	30.25	28.31	<b>25.19</b>	27.69	28.37	28.69
	$w\ell_1$ -norm	29.16	29.21	31.83	30.54	28.07	24.82	27.81	28.53	28.74
	$w\ell_p$ -norm	<b>29.29</b>	<b>29.28</b>	<b>31.85</b>	<b>30.56</b>	<b>28.39</b>	25.13	<b>27.84</b>	<b>28.62</b>	<b>28.87</b>
60%	$\ell_1$ -norm	29.61	29.82	32.29	30.78	29.02	25.93	28.53	28.93	29.36
	$\ell_p$ -norm	29.85	30.16	32.51	31.14	29.22	26.13	28.69	29.16	29.61
	$w\ell_1$ -norm	31.44	31.40	33.65	32.93	30.42	27.04	29.74	30.27	30.86
	$w\ell_p$ -norm	<b>31.46</b>	<b>31.54</b>	<b>33.67</b>	<b>33.02</b>	<b>30.56</b>	<b>27.21</b>	<b>29.77</b>	<b>30.35</b>	<b>30.95</b>
50%	$\ell_1$ -norm	31.62	31.45	33.78	32.62	30.68	27.64	30.13	30.48	31.05
	$\ell_p$ -norm	31.88	31.78	33.97	32.99	30.89	27.86	30.28	30.70	31.29
	$w\ell_1$ -norm	33.98	33.16	<b>35.30</b>	34.99	32.38	29.12	31.31	31.88	32.76
	$w\ell_p$ -norm	<b>34.00</b>	<b>33.26</b>	35.25	<b>35.05</b>	<b>32.53</b>	<b>29.26</b>	<b>31.32</b>	<b>31.91</b>	<b>32.82</b>

TABLE VI

PSNR (dB) COMPARISON OF  $\ell_1$ -NORM,  $\ell_p$ -NORM,  $w\ell_1$ -NORM AND  $w\ell_p$ -NORM, BASED ON THE ADAPTIVE DICTIONARY LEARNING SCHEME FOR IMAGE CS RECOVERY.

Ratio	Methods	Barbara	bridge	elaine	Fence	House	lena	peppers	straw	Average
0.2	$\ell_1$ -norm	32.24	25.03	34.59	29.31	36.01	30.77	30.00	24.11	30.26
	$\ell_p$ -norm	34.31	25.13	35.75	29.99	<b>37.15</b>	31.50	30.79	24.82	31.18
	$w\ell_1$ -norm	34.53	25.04	<b>36.22</b>	30.19	<b>37.07</b>	31.49	31.22	24.82	31.32
	$w\ell_p$ -norm	<b>34.55</b>	<b>25.28</b>	36.00	<b>30.38</b>	36.92	<b>31.62</b>	<b>31.31</b>	<b>25.06</b>	<b>31.39</b>
0.3	$\ell_1$ -norm	34.49	26.49	36.76	31.16	37.94	32.97	31.93	26.11	32.23
	$\ell_p$ -norm	34.86	26.59	37.07	31.42	38.29	33.15	32.21	26.23	32.48
	$w\ell_1$ -norm	37.10	<b>27.25</b>	38.26	32.50	39.07	34.26	<b>33.39</b>	27.84	33.71
	$w\ell_p$ -norm	<b>37.23</b>	27.22	<b>38.30</b>	<b>32.53</b>	<b>39.23</b>	<b>34.29</b>	33.32	<b>27.89</b>	<b>33.75</b>
0.4	$\ell_1$ -norm	36.79	27.94	38.58	32.84	39.70	34.76	33.63	27.95	34.02
	$\ell_p$ -norm	37.15	28.06	38.87	33.09	39.98	34.95	33.90	28.09	34.26
	$w\ell_1$ -norm	39.04	<b>28.90</b>	40.03	<b>34.50</b>	40.82	36.58	<b>35.10</b>	<b>30.30</b>	35.66
	$w\ell_p$ -norm	<b>39.13</b>	28.85	<b>40.05</b>	34.42	<b>40.93</b>	<b>36.66</b>	35.00	30.28	<b>35.67</b>
0.5	$\ell_1$ -norm	38.80	29.38	40.26	34.50	41.27	36.56	35.18	29.88	35.73
	$\ell_p$ -norm	39.19	29.51	40.54	34.75	41.52	36.78	35.43	30.07	35.97
	$w\ell_1$ -norm	40.84	30.51	41.52	<b>36.29</b>	42.25	38.99	<b>36.56</b>	<b>32.49</b>	37.43
	$w\ell_p$ -norm	<b>40.94</b>	<b>30.52</b>	<b>41.63</b>	36.24	<b>42.38</b>	<b>39.09</b>	36.53	32.46	<b>37.47</b>

TABLE VII

THE DETAILED INVOLVED PARAMETERS SETTING OF  $\rho$ ,  $\lambda$  FOR IMAGE INPAINTING AND IMAGE CS RECOVERY, BASED ON THE GRAPH-BASED DICTIONARY LEARNING METHOD [41] AND PCA DICTIONARY LEARNING METHOD [42], RESPECTIVELY.

Image Inpainting						
Graph	$\ell_1$ -norm		$\ell_p$ -norm		$w\ell_1$ -norm	$w\ell_p$ -norm
Parameters	$\rho$	$\lambda$	$\rho$	$\lambda$	$\rho$	$\rho$
80%	0.008	1e-5	0.003	7e-5	0.15	0.06
70%	0.003	1e-5	0.003	7e-5	0.1	0.05
60%	0.006	7e-5	0.003	5e-5	0.07	0.09
50%	0.003	7e-5	0.003	9e-5	0.05	0.05
Image CS Recovery						
PCA	$\ell_1$ -norm		$\ell_p$ -norm		$w\ell_1$ -norm	$w\ell_p$ -norm
Parameters	$\rho$	$\lambda$	$\rho$	$\lambda$	$\rho$	$\rho$
0.2	0.03	1e-6	0.003	7e-5	0.09	0.07
0.3	0.008	1e-6	0.006	7e-5	0.07	0.09
0.4	0.008	1e-6	0.008	1e-5	0.05	0.05
0.5	0.008	1e-6	0.008	1e-5	0.05	0.05

method [41] and PCA dictionary learning method [42] for image inpainting and image CS recovery, respectively. For more details about the graph-based dictionary learning and PCA dictionary learning methods, please refer to [41] and [42], respectively. Similar to the proposed ADL dictionary, we learn the graph-based dictionary and PCA dictionary from

each group of the degraded image for image inpainting and image CS recovery, respectively. All the parameters remained the same as specified in the subsection V-A except for  $\rho$  and  $\lambda$ . Table VII shows the detailed setting of the involved parameters  $\rho$  and  $\lambda$ . The PSNR comparison results for image inpainting among four competing methods are shown in Table VIII. It can be observed that the weighted  $\ell_p$ -norm consistently outperforms the other three norms based on all test images (the only exception is the image *Zebra* for which the weighted  $\ell_1$ -norm is slightly higher than the weighted  $\ell_p$ -norm in the scene of 80% and 70% pixels missing). The PSNR comparison results of image CS recovery are shown in Table IX, one can observe that the weighted  $\ell_p$ -norm outperforms the other three norms in most cases. Fig. 6 shows the visual comparison of image *Fence* with 80% pixels missing for image inpainting based on graph-based dictionary learning method. The visual comparison of image *peppers* with  $0.2N$  measurements for image CS recovery based on PCA dictionary learning method is shown in Fig. 7. It can be seen that the weighted  $\ell_p$ -norm achieves better visual quality than other three norms. Obviously, we use these two more general dictionary learning methods to further demonstrate the feasibility of the proposed

TABLE VIII  
PSNR (dB) COMPARISON OF  $\ell_1$ -NORM,  $\ell_p$ -NORM,  $w\ell_1$ -NORM AND  $w\ell_p$ -NORM, BASED ON THE GRAPH-BASED DICTIONARY LEARNING METHOD FOR IMAGE INPAINTING.

Miss pixels	Methods	Mickey	Butterfly	Fence	Starfish	Nanna	Zebra	fireman	Golem	Average
80%	$\ell_1$ -norm	24.63	23.62	22.92	26.27	25.52	20.45	24.59	23.57	23.82
	$\ell_p$ -norm	25.20	24.51	25.83	26.41	24.79	20.79	24.88	24.31	24.59
	$w\ell_1$ -norm	25.30	24.63	26.67	26.20	24.75	<b>20.98</b>	24.88	24.44	24.73
	$w\ell_p$ -norm	<b>25.40</b>	<b>24.74</b>	<b>26.99</b>	<b>26.43</b>	<b>24.92</b>	20.97	<b>25.00</b>	<b>24.60</b>	<b>24.88</b>
70%	$\ell_1$ -norm	26.31	25.75	25.06	28.07	26.21	21.84	26.08	25.33	25.58
	$\ell_p$ -norm	27.21	26.88	28.27	28.33	26.58	22.43	26.50	26.43	26.58
	$w\ell_1$ -norm	27.37	27.00	28.89	27.92	26.57	<b>22.80</b>	26.55	26.65	26.72
	$w\ell_p$ -norm	<b>27.49</b>	<b>27.19</b>	<b>29.12</b>	<b>28.50</b>	<b>26.81</b>	22.77	<b>26.77</b>	<b>26.84</b>	<b>26.93</b>
60%	$\ell_1$ -norm	27.58	27.50	27.48	29.46	27.61	23.37	27.38	26.80	27.15
	$\ell_p$ -norm	27.72	27.66	28.09	29.47	27.65	23.46	27.41	26.93	27.30
	$w\ell_1$ -norm	28.79	28.84	30.74	29.68	28.22	24.72	28.05	28.39	28.43
	$w\ell_p$ -norm	<b>28.80</b>	<b>28.91</b>	<b>30.79</b>	<b>29.80</b>	<b>28.29</b>	<b>24.75</b>	<b>28.11</b>	<b>28.45</b>	<b>28.49</b>
50%	$\ell_1$ -norm	29.14	29.24	29.73	30.93	29.12	24.84	28.78	28.37	28.77
	$\ell_p$ -norm	29.31	29.40	30.24	30.85	29.12	24.98	28.80	28.50	28.90
	$w\ell_1$ -norm	30.68	30.62	32.65	31.51	29.76	26.61	29.64	30.04	30.19
	$w\ell_p$ -norm	<b>30.71</b>	<b>30.69</b>	<b>32.71</b>	<b>31.56</b>	<b>29.82</b>	<b>26.62</b>	<b>29.70</b>	<b>30.08</b>	<b>30.24</b>

TABLE IX  
PSNR (dB) COMPARISON OF  $\ell_1$ -NORM,  $\ell_p$ -NORM,  $w\ell_1$ -NORM AND  $w\ell_p$ -NORM, BASED ON PCA DICTIONARY LEARNING SCHEME FOR IMAGE CS RECOVERY.

Ratio	Methods	Barbara	bridge	elaine	Fence	House	lena	peppers	straw	Average
0.2	$\ell_1$ -norm	32.13	25.05	34.60	29.12	35.92	30.78	30.08	24.10	30.22
	$\ell_p$ -norm	34.07	25.24	<b>35.74</b>	29.87	<b>36.76</b>	31.46	30.87	24.74	31.09
	$w\ell_1$ -norm	32.89	25.25	33.32	29.87	36.23	31.23	31.10	24.50	30.55
	$w\ell_p$ -norm	<b>34.09</b>	<b>25.29</b>	35.74	<b>30.14</b>	36.75	<b>31.48</b>	<b>31.31</b>	<b>24.89</b>	<b>31.21</b>
0.3	$\ell_1$ -norm	34.38	26.53	36.80	31.08	38.05	33.03	32.10	26.09	32.26
	$\ell_p$ -norm	34.50	26.59	36.84	31.19	38.04	33.09	32.24	26.18	32.33
	$w\ell_1$ -norm	35.53	26.95	34.94	31.73	38.04	33.69	32.99	27.05	32.61
	$w\ell_p$ -norm	<b>35.69</b>	<b>27.04</b>	<b>37.25</b>	<b>31.84</b>	<b>38.07</b>	<b>33.80</b>	<b>33.06</b>	<b>27.28</b>	<b>33.01</b>
0.4	$\ell_1$ -norm	36.69	28.01	38.64	32.84	39.80	34.83	33.85	27.96	34.08
	$\ell_p$ -norm	37.02	28.13	38.92	33.09	<b>40.07</b>	35.04	34.10	28.09	34.31
	$w\ell_1$ -norm	37.62	28.39	39.03	33.43	39.75	35.46	34.59	29.07	34.67
	$w\ell_p$ -norm	<b>37.74</b>	<b>28.45</b>	<b>39.11</b>	<b>33.51</b>	39.84	<b>35.57</b>	<b>34.65</b>	<b>29.21</b>	<b>34.76</b>
0.5	$\ell_1$ -norm	38.72	29.46	40.32	34.55	41.36	36.64	35.45	29.89	35.80
	$\ell_p$ -norm	39.09	29.60	40.59	34.80	<b>41.59</b>	36.88	35.66	30.07	36.03
	$w\ell_1$ -norm	39.53	29.95	40.59	35.13	41.25	37.45	36.09	31.16	36.39
	$w\ell_p$ -norm	<b>39.64</b>	<b>30.00</b>	<b>40.67</b>	<b>35.21</b>	41.33	<b>37.56</b>	<b>36.14</b>	<b>31.30</b>	<b>36.48</b>

scheme.

### C. Comparison with the State-of-the-Arts

In this subsection, we validate the performance of the proposed scheme, i.e., group-based sparse coding with non-convex weighted  $\ell_p$ -norm (GSC- $w\ell_p$ ) minimization for image inpainting and image CS recovery with the proposed adaptive dictionary learning method. We compare the proposed GSC- $w\ell_p$  with recent state-of-the-art methods.

In image inpainting, we have compared the proposed GSC- $w\ell_p$  with five other competing methods: SALSA method [43], BPFA method [44], IPPO method [45], JSM method [46] and Aloha method [47]. Table X lists the PSNR comparison results for a collection of 8 color images among five competing methods. The average gain of the proposed GSC- $w\ell_p$  over SALSA, BPFA, IPPO, JSM and Aloha methods can be as much as 4.06dB, 2.26dB, 1.06dB, 1.25dB and 1.62dB, respectively. The visual comparison of image *Zebra* with 80% pixels missing is shown in Fig. 8. It can be seen that SALSA and BPFA could not reconstruct sharp edges and fine details. The IPPO, JSM and Aloha methods produce images with a much better visual quality than SALSA and BPFA, but still suffer from

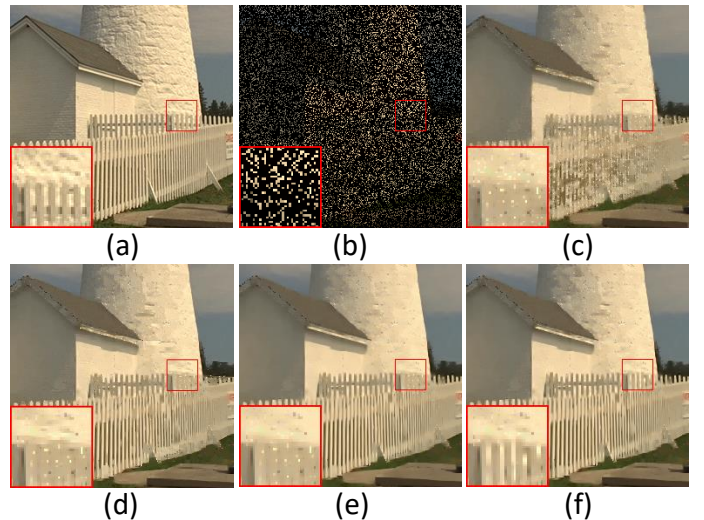


Fig. 6. Inpainting performance comparison on the image *Fence* based on the graph-based dictionary learning method. (a) Original image; (b) Degraded image with 80% pixels missing sample; (c)  $\ell_1$ -norm (PSNR= 22.92dB); (d)  $\ell_p$ -norm (PSNR= 25.83dB); (e)  $w\ell_1$ -norm (PSNR= 26.67dB); (f)  $w\ell_p$ -norm (PSNR= 26.99dB).

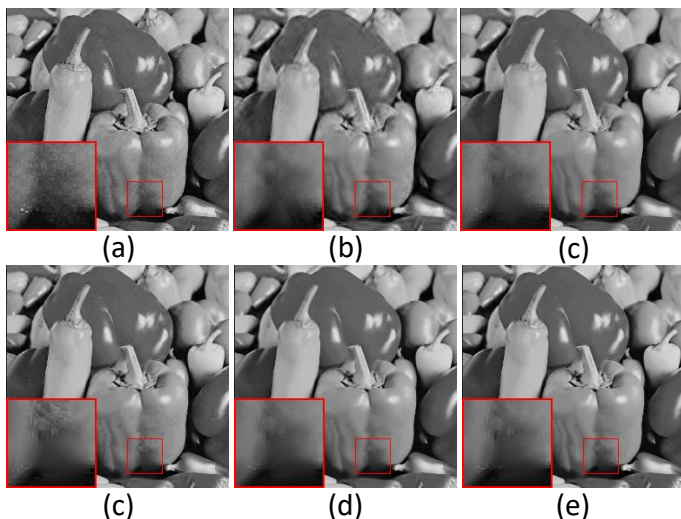


Fig. 7. CS recovery performance comparison on the image *peppers* based on PCA dictionary learning method. (a) Original image; (b) Initial image by [29] (PSNR= 28.61dB); (c)  $\ell_1$ -norm (PSNR= 30.08dB); (d)  $\ell_p$ -norm (PSNR= 30.87dB); (e)  $w\ell_1$ -norm (PSNR= 31.10dB); (f)  $w\ell_p$ -norm (PSNR= 31.31dB).

some undesirable artifacts, such as the ringing effects. The proposed  $GSC-w\ell_p$  not only preserves sharper edges and finer details, but eliminates the ringing effects.

In image CS recovery, we have compared the proposed  $GSC-w\ell_p$  based image CS recovery against six other competing methods including BCS method [48], BM3D-CS method [49], ADS-CS method [50], ALSB method [51], SGSR method [52] and MRK method [53]. The PSNR results are shown in Table XI. The proposed  $GSC-w\ell_p$  achieves 6.08dB, 1.95dB, 0.27dB, 1.33dB, 1.01dB and 1.59dB improvement on average over the BCS, BM3D-CS, ADS-CS, ALSB, SGSR and MRK, respectively. The visual comparison of image *Barbara* with  $0.2N$  measurements is shown in Fig. 9. One can observe that the BCS method generates the worst perceptual result. The BM3D-CS, ADS-CS, ALSB, SGSR and MRK methods still suffer from some undesirable artifacts or over-smooth phenomena. By contrast, the proposed  $GSC-w\ell_p$  not only removes most of the visual artifacts, but also preserves large-scale sharp edges and small-scale fine image details more effectively.

#### D. Effect of the number of the best matched patches

In this subsection, we have discussed how to select the best matching patch numbers  $m$  for the performance of the proposed  $GSC-w\ell_p$ . Specifically, to investigate the sensitivity of our method against  $m$ , two experiments were conducted with respect to different  $m$ , ranging from 20 to 200, in the case of image inpainting with 70% pixels missing and image CS recovery with  $0.2N$  measurements, respectively. The results with different  $m$  as shown in Fig. 10. It can be seen that all the curves are almost flat, showing the performance of the proposed  $GSC-w\ell_p$  is insensitive to  $m$ . The best performance of each case was usually achieved with  $m$  in the range [40,80]. Therefore, in this paper  $m$  was empirically set to be 60.

#### E. Comparison Between ADMM and IST

In this subsection, another classical optimization method iterative shrinkage/thresholding (IST) [54] is exploited to solve the proposed  $GSC-w\ell_p$  of Eq. (18) for CS image reconstruction. We will make a comparison between ADMM and IST with ratio = 0.2 and ratio= 0.3 for two image *elaine* and *Barbara* as examples, respectively. Fig. 11 shows their progression curves of the PSNR (dB) results achieved by ADMM and IST, respectively. It is obvious that ADMM algorithm is more fast efficient and effective to solve the proposed  $GSC-w\ell_p$  than IST algorithm.

#### F. Convergence

Since the proposed model is non-convex, it is difficult to give its theoretical proof for global convergence. Here, we only provide empirical evidence to display the good convergence of the proposed model. Fig. 12 illustrates the convergence performance of the proposed scheme. It shows the curves of the PSNR values versus the iteration numbers for image CS with  $0.2N$  measurements as well as image inpainting with 80% pixels missing, respectively. It can be seen that with the increase of the iteration number, the PSNR curves of the reconstructed images gradually increase and become flat and stable. Therefore, the proposed scheme has a good convergence performance.

## VI. CONCLUSION

This paper analyzed the group sparsity based on the rank minimization methods. An adaptive dictionary learning method for each group was designed, ensuring a low computational complexity. We proved the equivalence of the group-based sparse coding and the rank minimization problem, and thus the sparse coefficients of each group were measured by computing the singular values of each group. In this way, we have a benchmark to measure the sparsity of each group since its singular values can be easily computed by SVD operator. Four nuclear norm minimization methods including NNM, SNM, WNNM and WSNM were used to analyze the sparsity of each group and the solution of WSNM was the best approximation to real singular values of each group. Therefore, WSNM can be equivalently transformed into a non-convex weighted  $\ell_p$ -norm minimization problem in group-based sparse coding. To make the proposed scheme tractable and robust, we exploited the alternating direction method of multipliers (ADMM) to solve non-convex weighted  $\ell_p$ -norm minimization problem. Experimental results on two low-level studies, image inpainting and image CS recovery, have demonstrated that the proposed scheme is feasible and achieves performance improvements over the current state-of-the-art methods both quantitatively and qualitatively.

TABLE X  
PSNR (dB) COMPARISON OF SALSA [43], BPFA [44], IPPO [45], JSM [46], ALOHA [47] AND GSC- $wl_p$ .

Miss pixels	Methods	Mickey	Butterfly	Fence	Starfish	Nanna	Zebra	fireman	Golem	Average
80%	SALSA [43]	24.46	22.85	21.80	25.70	24.12	19.68	24.38	23.15	23.27
	BPFA [44]	24.53	24.04	26.24	26.79	24.71	20.90	24.88	24.13	24.52
	IPPO [45]	26.33	25.13	27.98	26.30	25.60	22.71	25.56	25.66	25.66
	JSM [46]	26.09	25.57	28.59	27.07	25.33	21.88	25.31	25.40	25.65
	Aloha [47]	25.33	24.88	28.88	26.33	25.54	22.72	25.03	25.23	25.49
	GSC- $wl_p$	<b>26.92</b>	<b>26.52</b>	<b>30.00</b>	<b>28.05</b>	<b>25.95</b>	<b>23.06</b>	<b>25.80</b>	<b>26.26</b>	<b>26.57</b>
70%	SALSA [43]	25.98	25.06	23.57	27.55	25.44	21.41	25.82	25.00	24.98
	BPFA [44]	26.16	26.68	28.87	28.93	26.62	22.78	26.55	26.46	26.63
	IPPO [45]	28.59	27.68	30.08	28.91	27.44	24.76	27.44	27.92	27.85
	JSM [46]	28.25	27.97	30.46	29.36	27.34	23.95	27.16	27.59	27.76
	Aloha [47]	27.11	27.29	30.57	28.22	27.43	24.55	26.52	27.33	27.38
	GSC- $wl_p$	<b>29.29</b>	<b>29.28</b>	<b>31.85</b>	<b>30.56</b>	<b>28.39</b>	<b>25.13</b>	<b>27.84</b>	<b>28.61</b>	<b>28.87</b>
60%	SALSA [43]	27.41	26.79	25.45	29.09	26.94	22.80	27.15	26.66	26.54
	BPFA [44]	27.83	28.88	30.79	30.98	28.63	24.53	28.23	28.30	28.52
	IPPO [45]	30.76	29.85	32.14	31.09	29.41	26.79	29.13	29.57	29.84
	JSM [46]	29.85	29.83	32.23	31.40	29.09	25.90	28.79	29.24	29.54
	Aloha [47]	28.59	29.16	32.33	30.19	29.51	26.24	28.24	28.92	29.15
	GSC- $wl_p$	<b>31.46</b>	<b>31.54</b>	<b>33.67</b>	<b>33.02</b>	<b>30.56</b>	<b>27.21</b>	<b>29.77</b>	<b>30.35</b>	<b>30.95</b>
50%	SALSA [43]	28.98	28.52	27.25	30.90	28.52	24.42	28.54	28.20	28.17
	BPFA [44]	29.43	30.98	32.82	33.13	30.68	26.37	30.12	30.46	30.50
	IPPO [45]	32.74	31.69	33.95	33.10	31.17	28.42	30.82	31.11	31.63
	JSM [46]	31.96	31.47	33.75	33.24	30.75	27.77	30.37	30.89	31.27
	Aloha [47]	30.33	30.78	33.79	31.85	31.24	27.67	29.88	30.28	30.73
	GSC- $wl_p$	<b>34.00</b>	<b>33.26</b>	<b>35.25</b>	<b>35.05</b>	<b>32.53</b>	<b>29.26</b>	<b>31.32</b>	<b>31.91</b>	<b>32.82</b>

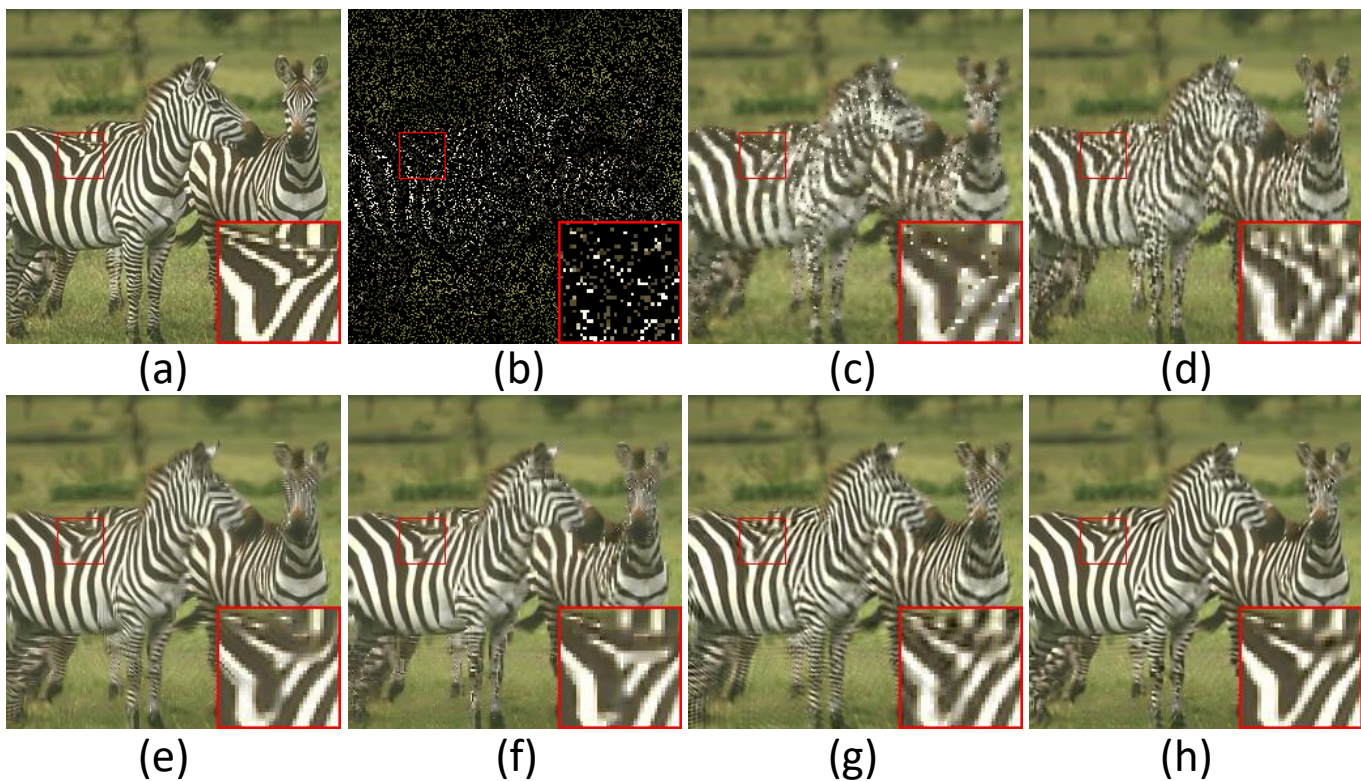


Fig. 8. Inpainting performance comparison on the image Zebra. (a) Original image; (b) Degraded image with 80% pixels missing sample; (c) SALSA [43] (PSNR= 19.68dB); (d) BPFA [44] (PSNR= 20.90dB); (e) IPPO [45] (PSNR= 22.71dB); (f) JSM [46] (PSNR= 21.88dB); (g) Aloha [47] (PSNR=22.72dB); (h) GSC- $wl_p$  (PSNR= 23.06dB).

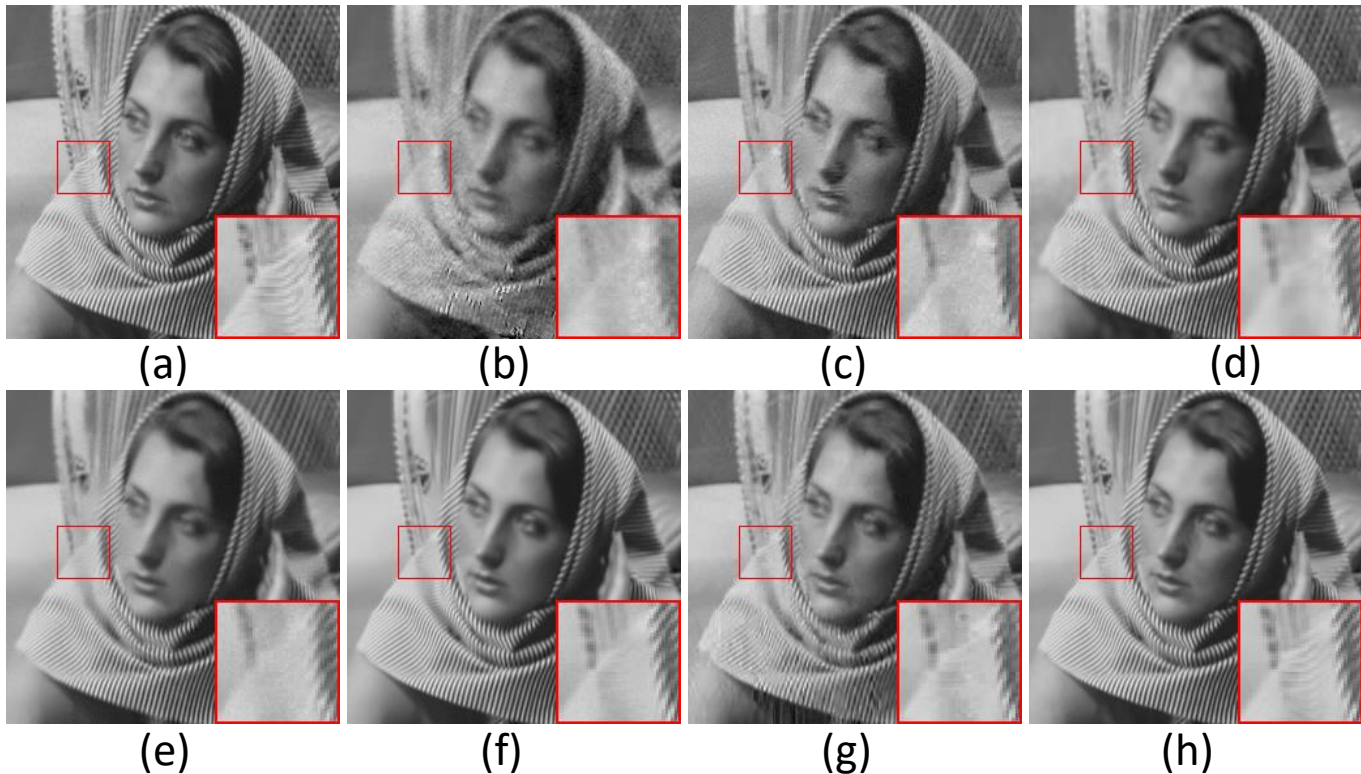


Fig. 9. CS recovery image *Barbara* with  $0.2N$  measurements. (a) Original image; (b) BCS [48] (PSNR =24.24dB); (c) BM3D-CS [49] (PSNR= 28.83dB); (d) ADS-CS [50] (PSNR= 32.27dB); (e) ALSB [51] (PSNR= 30.72dB); (f) SGSR [52] (PSNR= 33.44dB); (g) MRK [53] (PSNR= 27.99dB); (h) GSC- $wl_p$  (PSNR= 34.55dB).

TABLE XI  
PSNR (dB) COMPARISON OF BCS [48], BM3D-CS [49], ADS-CS [50], ALSB [51], SGSR [52], MRK [53] AND GSC- $wl_p$ .

Ratio	Methods	Barbara	bridge	elaine	Fence	House	lena	peppers	straw	Average
0.2	BCS [48]	24.24	23.61	31.18	21.57	30.54	28.15	27.15	20.69	25.89
	BM3D-CS [49]	28.83	23.77	33.75	22.57	35.04	30.30	31.09	20.04	28.17
	ADS-CS [50]	32.27	25.39	35.78	28.37	35.76	33.92	31.01	23.74	30.78
	ALSB [51]	30.72	24.97	32.56	28.41	36.08	30.68	29.96	24.33	29.71
	SGSR [52]	33.44	24.72	34.85	29.42	35.81	30.89	30.51	24.54	30.52
	MRK [53]	27.99	<b>25.70</b>	35.94	22.20	36.36	<b>32.58</b>	<b>31.83</b>	23.02	29.45
	GSC- $wl_p$	<b>34.55</b>	25.28	<b>36.00</b>	<b>30.37</b>	<b>36.91</b>	31.62	31.32	<b>25.06</b>	<b>31.39</b>
0.3	BCS [48]	25.59	25.00	33.68	23.24	32.85	30.16	29.05	22.19	27.72
	BM3D-CS [49]	33.00	26.59	37.23	30.68	36.84	35.01	33.62	22.37	31.92
	ADS-CS [50]	35.81	27.36	37.91	31.29	38.21	37.20	33.26	26.58	33.45
	ALSB [51]	35.00	26.83	34.30	30.83	38.34	33.36	32.37	26.61	32.21
	SGSR [52]	35.91	26.80	36.87	31.56	37.37	33.27	32.71	27.33	32.73
	MRK [53]	32.64	<b>27.62</b>	38.40	24.44	38.35	<b>35.69</b>	<b>33.91</b>	25.52	32.07
	GSC- $wl_p$	<b>37.23</b>	27.22	<b>38.30</b>	<b>32.53</b>	<b>39.23</b>	34.29	33.32	<b>27.89</b>	<b>33.75</b>
0.4	BCS [48]	27.10	26.31	35.66	24.81	34.65	32.06	30.77	23.71	29.38
	BM3D-CS [49]	35.92	28.52	39.23	33.83	38.08	38.46	35.20	24.38	34.20
	ADS-CS [50]	38.34	29.10	39.60	34.02	40.30	39.63	34.96	28.80	35.59
	ALSB [51]	38.34	29.10	39.60	32.83	40.25	35.47	34.44	28.54	34.58
	SGSR [52]	37.70	28.46	38.63	33.34	38.99	35.68	34.47	29.63	34.61
	MRK [53]	36.17	<b>29.24</b>	40.02	26.63	40.04	<b>38.14</b>	<b>35.50</b>	27.69	34.18
	GSC- $wl_p$	<b>39.13</b>	28.85	<b>40.05</b>	<b>34.42</b>	<b>40.93</b>	36.66	35.00	<b>30.28</b>	<b>35.67</b>
0.5	BCS [48]	28.67	27.64	37.51	26.20	36.29	33.78	32.31	25.30	30.96
	BM3D-CS [49]	38.43	30.68	41.01	36.21	40.34	39.19	36.80	26.94	36.20
	ADS-CS [50]	40.19	30.83	40.92	36.20	41.86	41.60	36.46	30.88	37.37
	ALSB [51]	39.26	30.03	41.18	34.81	41.93	37.79	36.21	30.61	36.48
	SGSR [52]	39.38	30.09	40.07	35.28	40.56	37.90	35.97	31.71	36.37
	MRK [53]	38.98	<b>31.01</b>	41.61	29.60	41.46	<b>39.99</b>	<b>36.97</b>	30.11	36.22
	GSC- $wl_p$	<b>40.94</b>	30.52	<b>41.63</b>	<b>36.24</b>	<b>42.38</b>	39.09	36.53	<b>32.46</b>	<b>37.47</b>

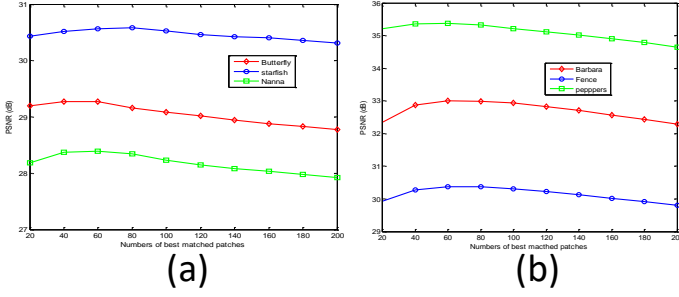


Fig. 10. Performance comparison with different matched patch numbers  $k$  for image CS recovery and image inpainting. (a) PSNR results achieved by different  $m$  in the case of the image inpainting with 70% missing sample. (b) PSNR results achieved by different  $m$  in the case of the image CS recovery with  $0.2N$  measurements.

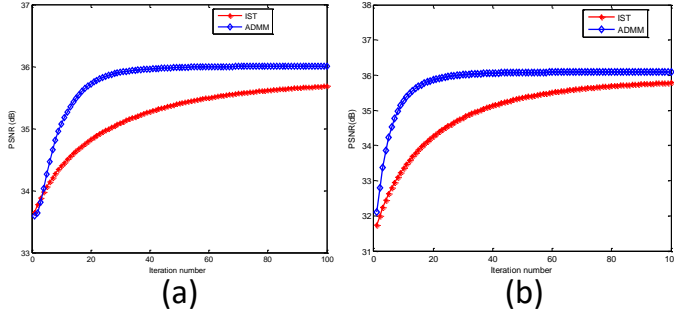


Fig. 11. Comparison between ADMM and IST. (a) PSNR results achieved by ADMM and IST with ratio = 0.2 for image *elaine*. (b) PSNR results achieved by ADMM and IST with ratio = 0.3 for image *Barbara*.

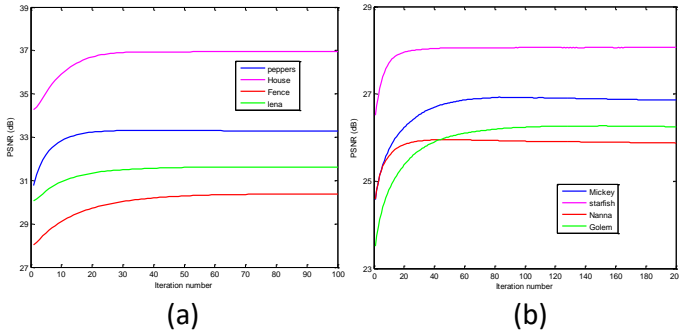


Fig. 12. Convergence analysis of the proposed scheme. (a) PSNR results versus iteration number for image CS recovery with  $0.2N$  measurements. (b) PSNR results versus iteration number for image inpainting with 80% pixels missing.

## APPENDIX A PROOF OF THE THEOREM 1

*Proof.* Since the adaptive dictionary  $\mathbf{D}_i$  is constructed by Eq. (9), and the unitary property of  $\mathbf{U}_i$  and  $\mathbf{V}_i$ , we have

$$\begin{aligned}
 \|\mathbf{Y}_i - \mathbf{X}_i\|_F^2 &= \|\mathbf{D}_i(\boldsymbol{\mu}_i - \boldsymbol{\alpha}_i)\|_F^2 = \|\mathbf{U}_i \text{diag}(\boldsymbol{\mu}_i - \boldsymbol{\alpha}_i) \mathbf{V}_i\|_F^2 \\
 &= \text{trace}(\mathbf{U}_i \text{diag}(\boldsymbol{\mu}_i - \boldsymbol{\alpha}_i) \mathbf{V}_i \mathbf{V}_i^T \text{diag}(\boldsymbol{\mu}_i - \boldsymbol{\alpha}_i) \mathbf{U}_i^T) \\
 &= \text{trace}(\mathbf{U}_i \text{diag}(\boldsymbol{\mu}_i - \boldsymbol{\alpha}_i) \text{diag}(\boldsymbol{\mu}_i - \boldsymbol{\alpha}_i) \mathbf{U}_i^T) \\
 &= \text{trace}(\text{diag}(\boldsymbol{\mu}_i - \boldsymbol{\alpha}_i) \mathbf{U}_i \mathbf{U}_i^T \text{diag}(\boldsymbol{\mu}_i - \boldsymbol{\alpha}_i)) \\
 &= \text{trace}(\text{diag}(\boldsymbol{\mu}_i - \boldsymbol{\alpha}_i) \text{diag}(\boldsymbol{\mu}_i - \boldsymbol{\alpha}_i)) \\
 &= \|\boldsymbol{\mu}_i - \boldsymbol{\alpha}_i\|_2^2
 \end{aligned} \tag{39}$$

## APPENDIX B PROOF OF THE THEOREM 2

*Proof.* On the basis of *Theorem 1*, we have

$$\begin{aligned}
 \boldsymbol{\alpha}_i &= \arg \min_{\boldsymbol{\alpha}_i} \left\{ \frac{1}{2} \|\mathbf{Y}_i - \mathbf{D}_i \boldsymbol{\alpha}_i\|_F^2 + \lambda \|\boldsymbol{\alpha}_i\|_1 \right\} \\
 &= \arg \min_{\boldsymbol{\alpha}_i} \left\{ \frac{1}{2} \|\boldsymbol{\gamma}_i - \boldsymbol{\alpha}_i\|_2^2 + \lambda \|\boldsymbol{\alpha}_i\|_1 \right\}
 \end{aligned} \tag{40}$$

Thus, based on *Lemma 1*, we have

$$\boldsymbol{\alpha}_i = \text{soft}(\boldsymbol{\gamma}_i, \lambda) = \text{sgn}(\boldsymbol{\gamma}_i, \lambda) \cdot \max(\text{abs}(\boldsymbol{\gamma}_i) - \lambda, 0) \tag{41}$$

Obviously, according to Eqs. (8) and (9), we have

$$\begin{aligned}
 \mathbf{D}_i \boldsymbol{\alpha}_i &= \sum_{j=1}^{n_1} \text{soft}(\boldsymbol{\gamma}_{i,j}, \lambda) \mathbf{d}_{i,j} \\
 &= \sum_{j=1}^{n_1} \text{soft}(\boldsymbol{\gamma}_{i,j}, \lambda) \mathbf{u}_{i,j} \mathbf{v}_{i,j}^T \\
 &= \mathbf{U}_i \mathcal{D}_\lambda(\boldsymbol{\Sigma}_i) \mathbf{V}_i^T
 \end{aligned} \tag{42}$$

where  $\boldsymbol{\alpha}_{i,j}$  represents the  $j$ -th element of the  $i$ -th group sparse coefficient  $\boldsymbol{\alpha}_i$ , and  $\boldsymbol{\Sigma}_i$  is the singular value matrix of the  $i$ -th group  $\mathbf{Y}_i$ .

Thus, based on *Lemma 2*, we prove that the group-based sparse coding (Eq. (15)) is equivalent to the rank minimization problem (Eq. (14)).  $\square$

## APPENDIX C PROOF OF THE THEOREM 3

*Proof.* Owing to the assumption that  $\mathbf{e}(\mathbf{j})$  follows an independent zero mean distribution with variance  $\sigma^2$ , namely,  $\mathbf{E}[\mathbf{e}(\mathbf{j})] = 0$  and  $\text{Var}[\mathbf{e}(\mathbf{j})] = \sigma^2$ . Thus, it can be deduced that each  $\mathbf{e}(\mathbf{j})^2$  is also independent, and the meaning of each  $\mathbf{e}(\mathbf{j})^2$  is:

$$\mathbf{E}[\mathbf{e}(\mathbf{j})^2] = \text{Var}[\mathbf{e}(\mathbf{j})] + [\mathbf{E}[\mathbf{e}(\mathbf{j})]]^2 = \sigma^2, j = 1, 2, \dots, N \tag{43}$$

By invoking the *law of Large numbers* in probability theory, for any  $\epsilon > 0$ , it leads to  $\lim_{N \rightarrow \infty} \mathbf{P}\{|\frac{1}{N} \sum_{j=1}^N \mathbf{e}(\mathbf{j})^2 - \sigma^2| < \frac{\epsilon}{2}\} = 1$ , namely,

$$\lim_{N \rightarrow \infty} \mathbf{P}\left\{ \left| \frac{1}{N} \|\mathbf{X} - \mathbf{R}\|_2^2 - \sigma^2 \right| < \frac{\epsilon}{2} \right\} = 1 \tag{44}$$

Next, we denote the concatenation of all the groups  $\mathbf{X}_i$  and  $\mathbf{R}_i$ ,  $i = 1, 2, \dots, n$ , by  $\mathbf{X}$  and  $\mathbf{R}$ , respectively. Meanwhile, we denote the error of each element of  $\mathbf{X} - \mathbf{R}$  by  $\mathbf{e}(s)$ ,  $s = 1, 2, \dots, S$ . We have also denote  $\mathbf{e}(s)$  following an independent zero mean distribution with variance  $\sigma^2$ .

Therefore, the same process applied to  $\mathbf{e}(s)^2$  yields  $\lim_{S \rightarrow \infty} \mathbf{P}\{|\frac{1}{S} \sum_{s=1}^S \mathbf{e}(s)^2 - \sigma^2| < \frac{\epsilon}{2}\} = 1$ , i.e.,

$$\lim_{S \rightarrow \infty} \mathbf{P}\left\{ \left| \frac{1}{S} \sum_{i=1}^n \|\mathbf{X}_i - \mathbf{R}_i\|_F^2 - \sigma^2 \right| < \frac{\epsilon}{2} \right\} = 1 \tag{45}$$

Obviously, considering Eqs. (44) and (45) together, we can prove Eq. (30).  $\square$

## REFERENCES

- [1] Aharon M, Elad M, Bruckstein A.  $k$ -SVD: An algorithm for designing overcomplete dictionaries for sparse representation[J]. IEEE Transactions on signal processing, 2006, 54(11): 4311-4322.
- [2] Elad M, Aharon M. Image denoising via sparse and redundant representations over learned dictionaries[J]. IEEE Transactions on Image processing, 2006, 15(12): 3736-3745.
- [3] Puthenpussery A, Liu Q, Liu C. A Sparse Representation Model Using the Complete Marginal Fisher Analysis Framework And Its Applications to Visual Recognition[J]. IEEE Transactions on Multimedia, 2017.
- [4] Liu Y, Zhai G, Gu K, et al. Reduced-reference Image Quality Assessment in Free-Energy Principle and Sparse Representation[J]. IEEE Transactions on Multimedia, 2017.
- [5] Mairal J, Bach F, Ponce J, et al. Online dictionary learning for sparse coding[C]//Proceedings of the 26th annual international conference on machine learning. ACM, 2009: 689-696.
- [6] Mairal J, Ponce J, Sapiro G, et al. Supervised dictionary learning[C]//Advances in neural information processing systems. 2009: 1033-1040.
- [7] Wen B, Ravishankar S, Bresler Y. Structured overcomplete sparsifying transform learning with convergence guarantees and applications[J]. International Journal of Computer Vision, 2015, 114(2-3): 137-167.
- [8] Ophir B, Lustig M, Elad M. Multi-scale dictionary learning using wavelets[J]. IEEE Journal of Selected Topics in Signal Processing, 2011, 5(5): 1014-1024.
- [9] Zhang Q, Li B. Discriminative K-SVD for dictionary learning in face recognition[C]//Computer Vision and Pattern Recognition (CVPR), 2010 IEEE Conference on. IEEE, 2010: 2691-2698.
- [10] Jiang Z, Lin Z, Davis L S. Label consistent K-SVD: Learning a discriminative dictionary for recognition[J]. IEEE Transactions on Pattern Analysis and Machine Intelligence, 2013, 35(11): 2651-2664.
- [11] Lun D P K. Robust fringe projection profilometry via sparse representation[J]. IEEE Transactions on Image Processing, 2016, 25(4): 1726-1739.
- [12] Mairal J, Bach F, Ponce J, et al. Non-local sparse models for image restoration[C]//Computer Vision, 2009 IEEE 12th International Conference on. IEEE, 2009: 2272-2279.
- [13] Zhang J, Zhao D, Gao W. Group-based sparse representation for image restoration[J]. IEEE Transactions on Image Processing, 2014, 23(8): 3336-3351.
- [14] Dong W, Shi G, Ma Y, et al. Image restoration via simultaneous sparse coding: Where structured sparsity meets gaussian scale mixture[J]. International Journal of Computer Vision, 2015, 114(2-3): 217-232.
- [15] Wang Q, Zhang X, Wu Y, et al. Non-Convex Weighted  $\ell_p$  Minimization based Group Sparse Representation Framework for Image Denoising[J]. IEEE Signal Processing Letters, 2017, PP(99):1-1.
- [16] Candes E J, Wakin M B, Boyd S P. Enhancing sparsity by reweighted  $\ell_1$  minimization[J]. Journal of Fourier analysis and applications, 2008, 14(5): 877-905.
- [17] Cands E J, Romberg J, Tao T. Robust uncertainty principles: Exact signal reconstruction from highly incomplete frequency information[J]. IEEE Transactions on information theory, 2006, 52(2): 489-509.
- [18] Cai J F, Cands E J, Shen Z. A singular value thresholding algorithm for matrix completion[J]. SIAM Journal on Optimization, 2010, 20(4): 1956-1982.
- [19] Gu S, Zhang L, Zuo W, et al. Weighted nuclear norm minimization with application to image denoising[C]//Proceedings of the IEEE Conference on Computer Vision and Pattern Recognition. 2014: 2862-2869.
- [20] Nie F, Huang H, Ding C H Q. Low-Rank Matrix Recovery via Efficient Schatten  $p$ -Norm Minimization[C]//AAAI. 2012.
- [21] Xie Y, Gu S, Liu Y, et al. Weighted Schatten  $p$ -norm minimization for image denoising and background subtraction[J]. IEEE transactions on image processing, 2016, 25(10): 4842-4857.
- [22] Zha Z, Liu X, Huang X, et al. Analyzing the group sparsity based on the rank minimization methods[C]//Multimedia and Expo (ICME), 2017 IEEE International Conference on. IEEE, 2017: 883-888.
- [23] Srebro N, Jaakkola T. Weighted low-rank approximations[C]//Proceedings of the 20th International Conference on Machine Learning (ICML-03). 2003: 720-727.
- [24] Eriksson A, Van Den Hengel A. Efficient computation of robust low-rank matrix approximations in the presence of missing data using the  $\ell_1$  norm[C]//Computer Vision and Pattern Recognition (CVPR), 2010 IEEE Conference on. IEEE, 2010: 771-778.
- [25] Zhao Q, Meng D, Xu Z, et al.  $\ell_1$ -Norm Low-Rank Matrix Factorization by Variational Bayesian Method[J]. IEEE transactions on neural networks and learning systems, 2015, 26(4): 825-839.
- [26] Mnih A, Salakhutdinov R R. Probabilistic matrix factorization[C]//Advances in neural information processing systems. 2008: 1257-1264.
- [27] Kong Y, Shao M, Li K, et al. Probabilistic Low-Rank Multitask Learning[J]. IEEE transactions on neural networks and learning systems, 2017.
- [28] Li C, Yin W, Zhang Y. Users guide for TVAL3: TV minimization by augmented lagrangian and alternating direction algorithms[J]. CAAM report, 2009, 20: 46-47.
- [29] Chen C, Tramel E W, Fowler J E. Compressed-sensing recovery of images and video using multihypothesis predictions[C]//Signals, Systems and Computers (ASILOMAR), 2011 Conference Record of the Forty Fifth Asilomar Conference on. IEEE, 2011: 1193-1198.
- [30] Zha Z, Liu X, Zhou Z, et al. Image denoising via group sparsity residual constraint[C]//Acoustics, Speech and Signal Processing (ICASSP), 2017 IEEE International Conference on. IEEE, 2017: 1787-1791.
- [31] Wen B, Ravishankar S, Bresler Y. FRISThipping and rotation invariant sparsifying transform learning and applications[J]. Inverse Problems, 2017, 33(074007): 074007.
- [32] Zhou M, Chen H, Ren L, et al. Non-parametric Bayesian dictionary learning for sparse image representations[C]//Advances in neural information processing systems. 2009: 2295-2303.
- [33] Dong W, Shi G, Li X, et al. Compressive sensing via nonlocal low-rank regularization[J]. IEEE Transactions on Image Processing, 2014, 23(8): 3618-3632.
- [34] Boyd S, Parikh N, Chu E, et al. Distributed optimization and statistical learning via the alternating direction method of multipliers[J]. Foundations and Trends? in Machine Learning, 2011, 3(1): 1-122.
- [35] Chartrand R, Wohlberg B. A nonconvex ADMM algorithm for group sparsity with sparse groups[C]//Acoustics, Speech and Signal Processing (ICASSP), 2013 IEEE International Conference on. IEEE, 2013: 6009-6013.
- [36] Zhao C, Zhang J, Ma S, et al. Nonconvex  $L_p$  nuclear norm based ADMM framework for compressed sensing[C]//Data Compression Conference (DCC), 2016. IEEE, 2016: 161-170.
- [37] Afonso M V, Bioucas-Dias J M, Figueiredo M A T. Fast image recovery using variable splitting and constrained optimization[J]. IEEE Transactions on Image Processing, 2010, 19(9): 2345-2356.
- [38] Avriel M. Nonlinear programming: analysis and methods[M]. Courier Corporation, 2003.
- [39] Zuo W, Meng D, Zhang L, et al. A generalized iterated shrinkage algorithm for non-convex sparse coding[C]//Proceedings of the IEEE international conference on computer vision. 2013: 217-224.
- [40] Chang S G, Yu B, Vetterli M. Adaptive wavelet thresholding for image denoising and compression[J]. IEEE transactions on image processing, 2000, 9(9): 1532-1546.
- [41] Hu W, Li X, Cheung G, et al. Depth map denoising using graph-based transform and group sparsity[C]//Multimedia Signal Processing (MMSp), 2013 IEEE 15th International Workshop on. IEEE, 2013: 001-006.
- [42] Dong W, Zhang L, Shi G, et al. Nonlocally centralized sparse representation for image restoration[J]. IEEE Transactions on Image Processing, 2013, 22(4): 1620-1630.
- [43] Afonso M V, Bioucas-Dias J M, Figueiredo M A T. An augmented Lagrangian approach to the constrained optimization formulation of imaging inverse problems[J]. IEEE Transactions on Image Processing, 2011, 20(3): 681-695.
- [44] Zhou M, Chen H, Paisley J, et al. Nonparametric Bayesian dictionary learning for analysis of noisy and incomplete images[J]. IEEE Transactions on Image Processing, 2012, 21(1): 130-144.
- [45] Ram I, Elad M, Cohen I. Image processing using smooth ordering of its patches[J]. IEEE transactions on image processing, 2013, 22(7): 2764-2774.
- [46] Zhang J, Zhao D, Xiong R, et al. Image restoration using joint statistical modeling in a space-transform domain[J]. IEEE Transactions on Circuits and Systems for Video Technology, 2014, 24(6): 915-928.
- [47] Jin K H, Ye J C. Annihilating filter-based low-rank Hankel matrix approach for image inpainting[J]. IEEE Transactions on Image Processing, 2015, 24(11): 3498-3511.
- [48] Mun S, Fowler J E. Block compressed sensing of images using directional transforms[C]//Image Processing (ICIP), 2009 16th IEEE International Conference on. IEEE, 2009: 3021-3024.
- [49] Egiazarian K, Foi A, Katkovnik V. Compressed sensing image reconstruction via recursive spatially adaptive filtering[C]//Image Processing, 2007. ICIP 2007. IEEE International Conference on. IEEE, 2007, 1: I-549-I-552.

- [50] Dong W, Shi G, Li X, et al. Image reconstruction with locally adaptive sparsity and nonlocal robust regularization[J]. *Signal Processing: Image Communication*, 2012, 27(10): 1109-1122.
- [51] Zhang J, Zhao C, Zhao D, et al. Image compressive sensing recovery using adaptively learned sparsifying basis via L0 minimization[J]. *Signal Processing*, 2014, 103: 114-126.
- [52] Zhang J, Zhao D, Jiang F, et al. Structural group sparse representation for image compressive sensing recovery[C]//*Data Compression Conference (DCC)*, 2013. IEEE, 2013: 331-340.
- [53] Canh T N, Dinh K Q, Jeon B. Multi-scale/multi-resolution Kronecker compressive imaging[C]//*Image Processing (ICIP)*, 2015 IEEE International Conference on. IEEE, 2015: 2700-2704.
- [54] Beck A, Teboulle M. Fast gradient-based algorithms for constrained total variation image denoising and deblurring problems[J]. *IEEE Transactions on Image Processing*, 2009, 18(11): 2419-2434.